2.4. Beamlines and Beam Transfers

The desired functionality of the Recycler ring requires the addition of three 8 GeV proton and antiproton transfer lines. These transfer lines are shown on the right side of figure 2.4.1. The MI-32 and MI-40 proton injection and abort lines are used during commissioning and tune-up. The MI-22 and MI-32 antiproton transfer lines between the Main Injector and the Recycler are used for normal Tevatron Collider operations.

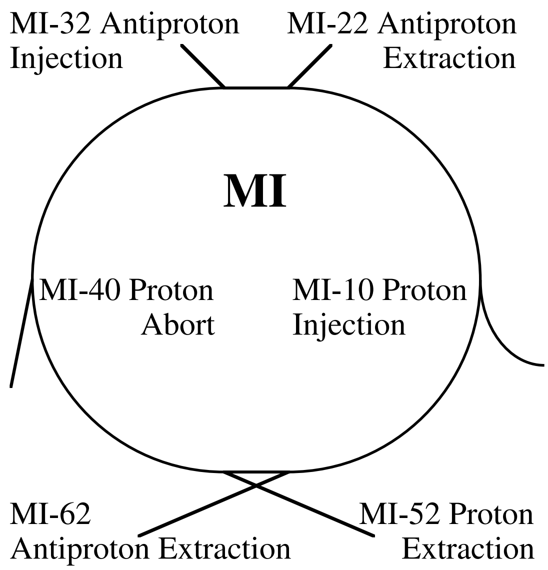

Figure 2.4.1: Sketch of the Main Injector (MI) and Recycler ring (RR) beam transfer lines. Note that the transfer lines at the MI-22 and MI-32 straight sections link the two rings together for injection and extraction of both antiprotons and protons.

2.4.1. Maximum Acceptable Kicker Ripple

The parameters which must be specified in order to design the kickers for these transfers are the kicker amplitude, rise/fall time, and flattop ripple magnitude. The allowed magnitude of kicker flattop ripple is determined by the amount of emittance growth which is considered acceptable. The equation describing the fractional emittance increase due to a position or angular misalignment normalized to the beam rms size or divergence respectively is

$$\frac{\varepsilon}{\varepsilon_o} = 1 + \tfrac{1}{2}\left(\frac{\Delta}{\sigma}\right)^2 \quad . \qquad (2.4.1)$$

According to equation (2.4.1) a given kicker amplitude error Δ causes more emittance growth $\varepsilon/\varepsilon_o$ as the initial beam divergence σ or emittance ε_o decreases. Using conservative numbers for the initial emittance and the acceptable level of emittance growth, table 2.4.1 displays the relevant parameters which determine the percentage kicker amplitude ripple or error. The dependence of emittance growth on kicker error is plotted in figure 2.4.2.

Table 2.4.1: Anticipated parameters dictating the acceptable level of kicker amplitude error or ripple during flattop.

Parameter	Value
Maximum emittance growth (95% Invariant π mmmr)	0.2
Minimum initial emittance (95% Invariant π mmmr)	10
Maximum kicker error / beam divergence (equation 2.4.1)	0.2
Beta function at the kicker magnet (m)	54
Minimum beam divergence at a kicker magnet (μrad)	57
Maximum deflection angle in a kicker (μrad)	12.0
Kicker amplitude in all transfer lines (mrad)	1.0
Maximum percentage kicker ripple/error magnitude (%)	±1.2

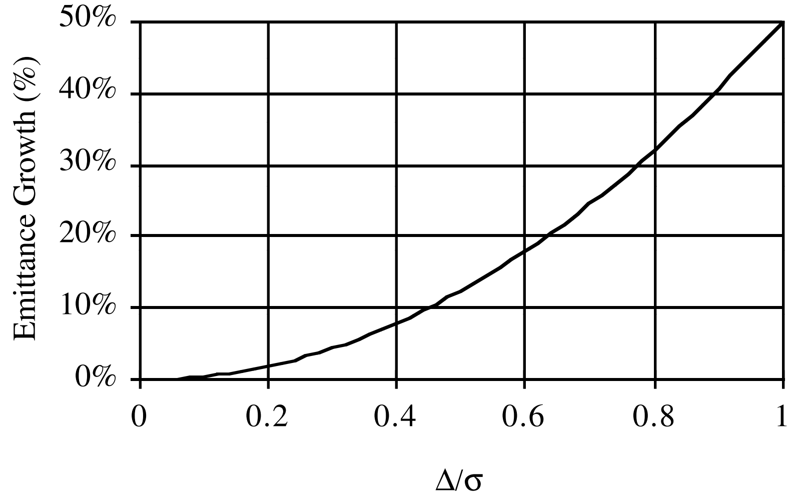

Figure 2.4.2: Fractional emittance growth as a function of the transfer angle or position error normalized to the rms beam divergence or size.

2.4.2. Role of Each Recycler Transfer Line

MI-32 Proton MI to RR: Used for commissioning and beam line tune-ups, the ability to easily inject protons into the Recycler from the Main Injector is necessary for efficient startup and operation. One positive aspect of the positioning of this transfer line is the fact that once the Main Injector is commissioned to its abort dump (which is the first half turn of the ring), Recycler commissioning can also start.

MI-40 Proton Abort: Used only during commissioning or other proton applications in which high intensities of beam can cause radiation safety or ground water activation problems, this abort line is basically identical to the Main Injector line. Since there is no emergency abort scenario envisioned, the kicker pulse length need only be 1.6 μsec in order to fulfill its ALARA mission. In the unlikely situation of multiple proton batch injection into the Recycler ring, multiple abort line transfers can be programmed to eliminate this beam. Figure 2.4.4 shows the geometry of this abort line showing the ring quadrupoles, the horizontal kicker, and the vertical Lambertson magnet.

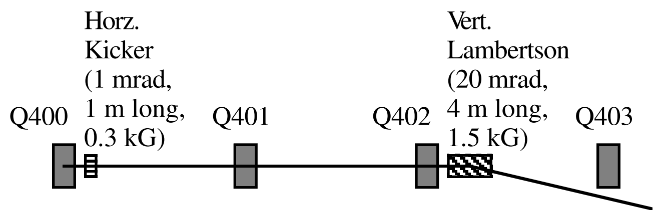

Figure 2.4.4: Elevation view of the Recycler ring MI-40 proton abort extraction geometry. The horizontal kicker deflects the extracted beam by 1 mrad into the bend field region of the vertical Lambertson magnet.

MI-22 Antiproton MI to RR: This transfer line directs antiprotons from the Main Injector and delivers them into a clockwise trajectory in the Recycler ring. The antiprotons are either enroute from the Accumulator or have been recycled from the Tevatron Collider. The maximum beam pulse length in either case is 1.6 μsec.

MI-32 Antiproton RR to MI: This transfer line directs cooled and formed antiprotons from the Recycler ring and delivers them into the Main Injector ready for acceleration and transfer into the Tevatron Collider. The kicker flattop must be at least 1.6 μsec.

2.4.3. Kicker and Lambertson Placement

In the Main Injector, it is possible to use the same kicker at MI-30 for both transfer lines at MI-32 and MI-22. By using a Recycler kicker at MI-20 for recycled antiproton injections at MI-22, the Recycler kicker at MI-22 away from any service buildings can be eliminated. This choice of kicker location is dictated by the fact that there is available space in that service building for the kicker hardware. Not only does the eliminate the civil construction cost of building a dedicated kicker building, but it also symmetrizes the two transfer lines about MI-30. As required, the betatron phase advance between the MI-20 and the MI-22 Lambertson is an odd multiple of 90°. Similarly, the kicker at MI-32 can be eliminated by using the MI-40 abort kicker. Therefore, the number of kickers is reduced from 6 to 3, a factor of 2 reduction. This scenario is sketched in figure 2.4.5. The advantages of this scheme are reduced cost and reduced Recycler ring impedance.

The details of the positioning of the MI-30 kicker in the Main Injector and the associated antiproton injection and extraction Lambertsons are sketched in figure 2.4.6. Since MI-22 and MI-32 are three half cell straight sections, the Main Injector Lambertsons are placed in those locations. In the Recycler there is so much free space between the gradient magnets that Lambertsons easily fit even in bend cells. The only catch is the leading gradient magnets at 216 and 328 need to be half (mirror) magnets in order for the extracted beam to clear with a 20 mrad kick.

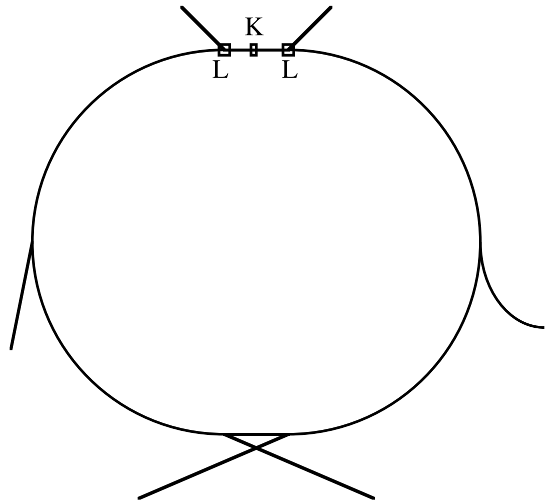

Figure 2.4.5: Sketches of the Main Injector (left) and Recycler ring (right) transfer lines in which only the new Lambertsons and kickers needed for Recycler ring operations are depicted. The displayed scenario assumes that kicker systems can be shared to service all of the transfer needs for a factor of 2 reduction in the number of systems.

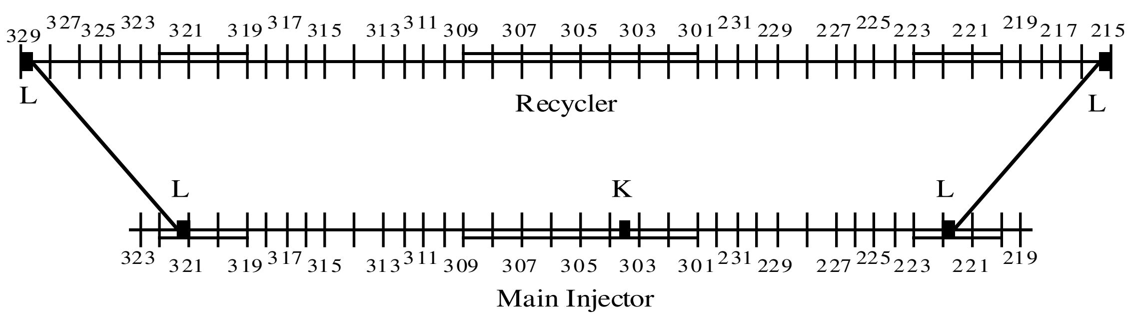

Figure 2.4.6: Sketch of the precise locations of the kickers and Lambertsons for the antiproton injection and extraction lines at MI-22 and MI-32.

Lattice designs and beam envelope calculations of the MI-22 and MI-32 transfer lines have been carried out [D. Johnson, MI Note 161]. The beam trajectories and full widths for the two machines and antiproton transfer directions are shown in figures 2.4.7 through 2.4.10. In figure 2.4.7 the antiproton recycling transfer from the Main Injector to the Recycler via MI-22 is shown from the point of view of the Main Injector. The closed orbit between the kicker and Lambertson is distorted with a pair of correction dipoles in order to optimize the use of horizontal aperture. The kicker launches the extracted beam on an opposite distortion which leads the beam into the Lambertson extraction channel. Both beams are assumed to have a transverse normalized 95% emittance of 40 π mmmr. The top and bottom of the plot are at the horizontal aperture of the Main Injector. In figure 2.4.8 the recycled antiprotons are shown in the Recycler ring just downstream of the injection Lambertson. In this case the horizontal aperture of the Recycler is explicitly indicated, and the beams are assumed to have an emittance of 20 π mmmr.

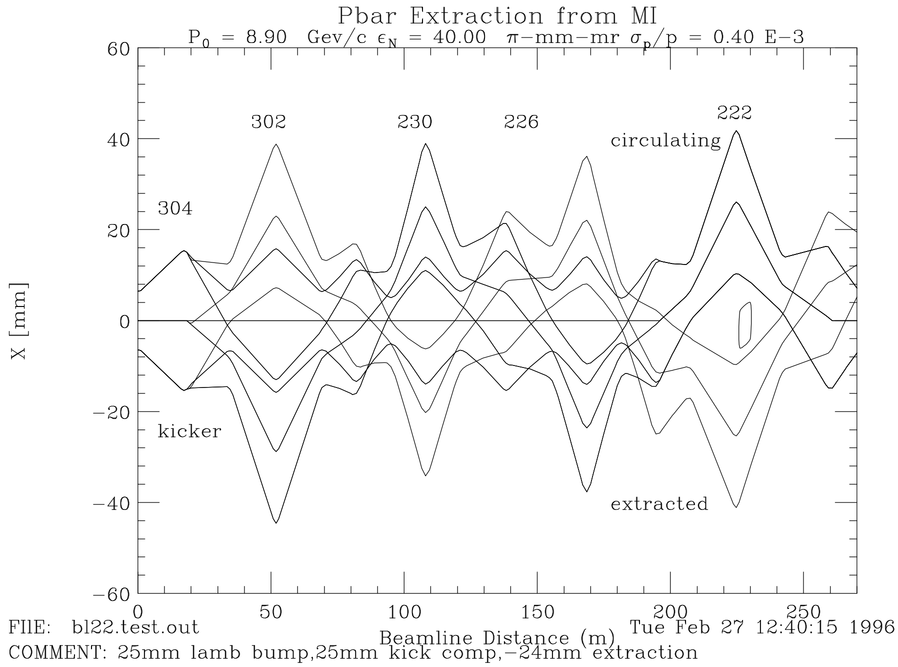

Figure 2.4.7: Beam trajectories and full widths of the stored and extracted beam in the Main Injector during antiproton recycling transfers from the Main Injector to the Recycler. The Main Injector horizontal aperture is at the extrema of the Y-axis of the plot.

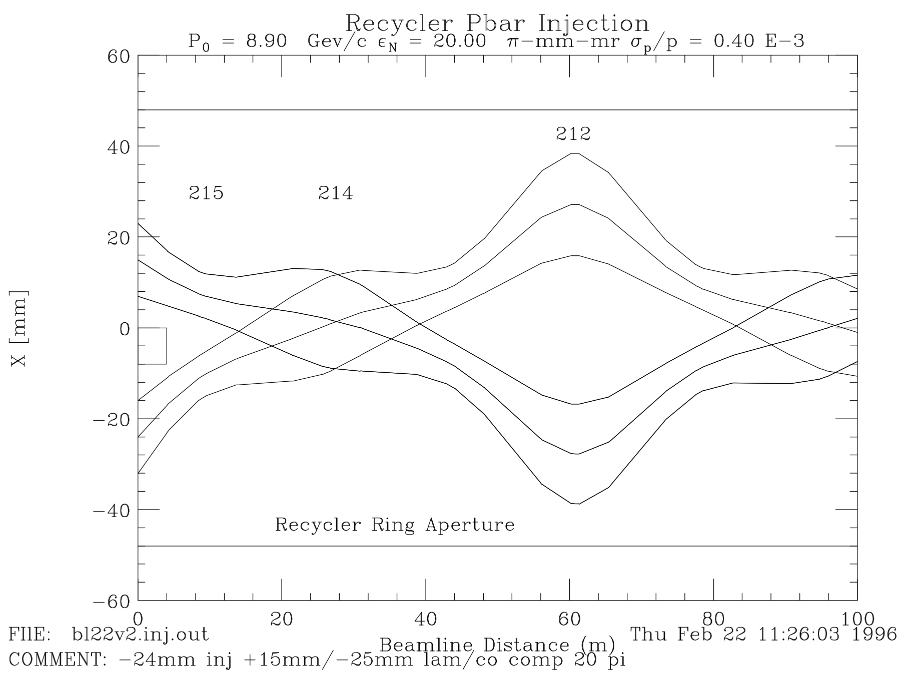

Figure 2.4.8: Beam trajectories and full widths of the stored and injected beam in the Recycler during antiproton recycling transfers from the Main Injector to the Recycler.

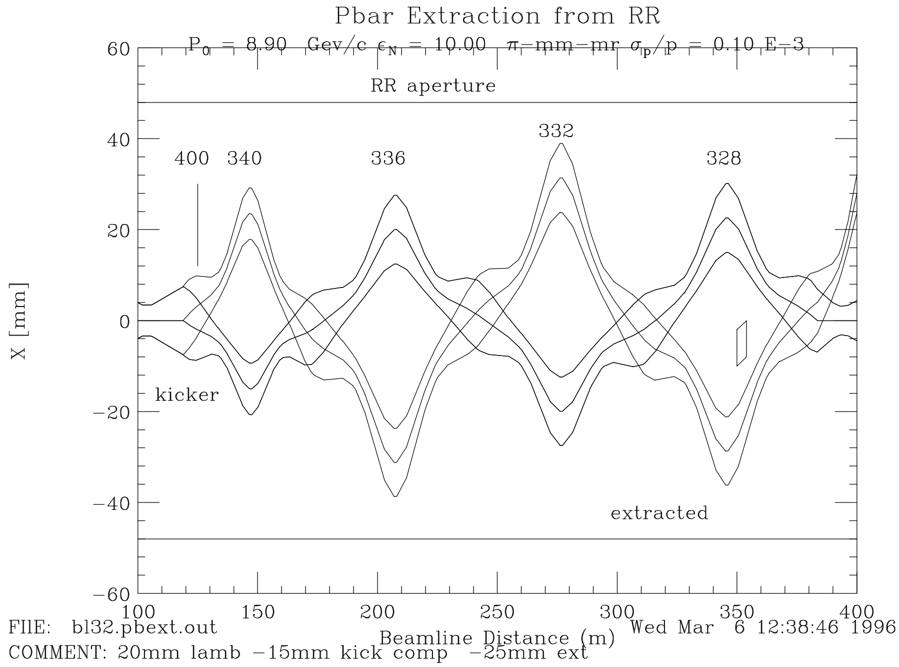

Figure 2.4.9: Beam trajectories and full widths of the stored and extracted beam in the Recycler during transfers of cooled antiprotons from the Recycler to the Main Injector.

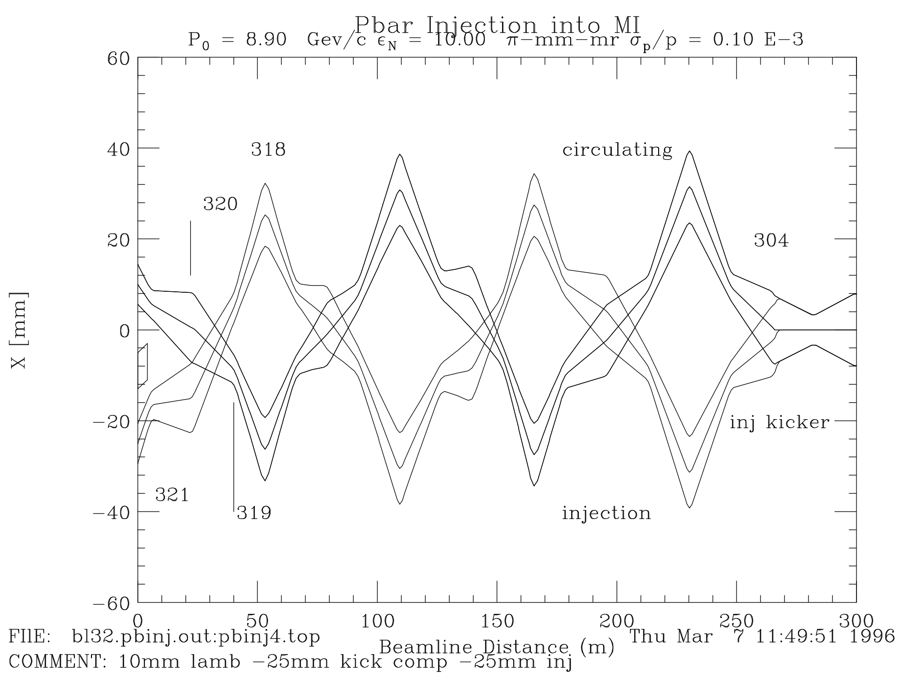

Figure 2.4.10: Beam trajectories and full widths of the stored and injected beam in the Main Injector during transfers of cooled antiprotons from the Recycler to the Main Injector. The Main Injector horizontal aperture is at the extrema of the Y-axis of the plot.

Extraction of cooled antiprotons from the Recycler for ultimate injection in the Tevatron Collider takes place via the MI-32 transfer line. In figure 2.4.9 the closed orbit and extracted beam orbits are shown between the kicker and Lambertson. A transverse normalized 95% emittance of 10 π mmmr was used to calculate the full beam widths of both the circulating and extracted beams. The beam trajectory and size after the transfer in the Main Injector is shown in figure 2.4.10.

2.4.4. Kicker and Lambertson Requirement Summary

In the transfer scenarios described in this design all kickers have an integrated kick of 300 Gauss-meters. The maximum kicker length in all of these scenarios is approximately 4 meters. In all cases the flattop duration of the kicker is at least 1.6 µsec. The rise and fall times for the two Recycler and one Main Injector kickers can be as large as 1-2 µsec. The minimum repetition interval for firing the kickers is anticipated to be 20 sec for antiproton transfers. Within the scope of Fermi III the proton injections are also limited to this interval.

In order to minimize the impedance effects of the two kickers in the Recycler, the beam tubes should be shielded or coated as much as possible. A reasonable criterion would be for the coating to slow down the rise and fall times by approximately 5-10%. Because of the slow rise times in these kickers, a rather thick coating can be used.

The Lambertsons are of the permanent magnet variety. Since there is a vertical correction magnet next to each vertically bending Lambertson, the tolerance on the field strength can be relaxed to as much as 1% (though in construction a manufacturing tolerance of 0.1% will be employed). The nominal bend angle of the Lambertsons is ±22 mrad.

2.4.5. Beam Synchronous Clocks and Beam Transfers

From the very beginning of accelerator operations at Fermilab, the transfers of beams from one accelerator to another has been complicated by the large number of transfer lines and beam dumps. As the years have gone by, especially with the addition of the Antiproton Source, the complexity of beam transfers has increased dramatically. With the addition of the Main Injector and Recycler, this trend definitely continues. Figure 2.4.11 contains a diagram of all of the beam destination options.

Since the advent of the Tevatron accelerator in the early 1980's, beam transfers between accelerators have generally taken advantage of beam synchronous clocks. Presently realized for the Main Ring and Tevatron, beam synchronous clock base frequencies are integer sub-harmonics of the machine RF (RF/7) while also synchronous with machine revolution frequency, each having 159 clock ticks per revolution. Similar in operation to TCLK, events exactly synchronous with a machine's revolution frequency (RF/1113) are coded onto each of these clocks and are denoted by the hexadecimal codes $\$AA_{MRBS}$ and $\$AA_{TVBS}$. The existing capability to transfer beam from any particular RF bucket of one machine to any particular bucket of another machine will be retained for the planned Recycler. Conceptually expressed, desired transfers between machines are allowed (or manipulated) to occur as the respective revolution events come into particular time (better stated as RF) alignment. Actual transfers are thereupon initiated by unique coded beam synchronous events that are placed constantly with respect to the revolution events. Required kicker timing is provided by beam sync timer modules that reference the unique transfer event and provide desired delay in machine revolutions and fractions thereof.

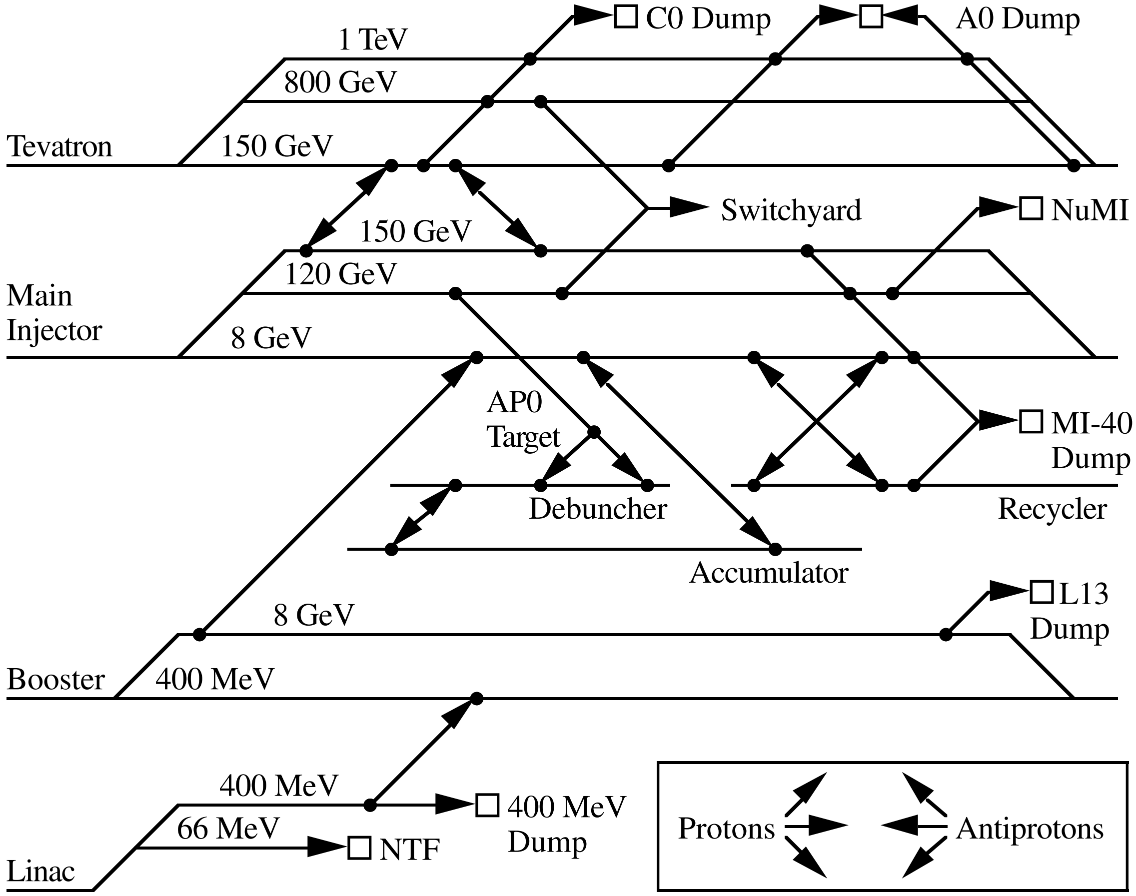

Figure 2.4.11: Map of all of the beam destination options at Fermilab after construction and commissioning of the Main Injector and the Recycler.

Transfers between the Recycler and Main Injector, which will require transfer cogging of the Main Injector RF, are relatively uncomplicated since the 53 MHz harmonic numbers of each machine both equal 588. Booster or Accumulator transfers to these larger machines are slightly more complicated in that their harmonic numbers are 84. However, transfers are simplified by the fact that the Booster and Accumulator harmonic numbers are exactly 1/7th that of the Recycler or Main Injector and that beam in either the Booster or Accumulator is, at least initially, uniformly distributed in longitudinal space.

The Recycler will require a new RF system and a derivative beam synchronous clock, RRBS, to facilitate beam transfers and circulating beam diagnostics. For this clock, $\$AA_{RRBS}$ is the assigned revolution marker event and there are 84 clock ticks per revolution. Development and installation of the new RRBS clock is judged as straight-forward in that RRBS architecture will largely duplicate that of other beam synchronous clocks. RRBS will be distributed from MI-60 to all Main Injector service buildings and to the Booster via fiber optic links.

Careful coordination of the Booster, Recycler, Main Injector, and Accumulator RF systems is fundamental to achieving successful transfers of beam. The fundamental 53 MHz reference of the Recycler RF system is to be considered as a fixed reference at 8 GeV to which other systems transfer cog and phase lock. While the operation of the Accumulator RF system has historically been independent, better synchronism strategies with the Main Injector need to be developed. The Recycler RF system will routinely provide appropriate barrier buckets for acceptance of beam while also partitioning fractions of circulating beam for extraction.

2.4.6. Beam Synchronous Transfer Events

A variety of new beam sync transfer events have been designated to effect desired transfers of particle beams to and from the Recycler. These events are temporally denoted by $\$Sn_{xxBS}$, with n ranging up from one, and with the subscript denoting the specific beam sync clock. Proper generation of these events ties closely with Recycler operating scenarios previously described and the TCLK resource. Details relative to the assignment and generation of these events are described hereafter. Discussion is facilitated by first describing the general sequence of TCLK and beam sync events on a per scenario basis. BES denotes the "Booster Extraction Sync" pulse signal presently generated by the Booster low-level RF timing hardware. It is also worthwhile to note that all beam sync transfer events are detected and mirrored as TCLK events with typical related time skew of 100 nanoseconds or less. This mirroring of beam synchronous transfer events in the Tevatron Clock has proven useful for diagnostic purposes.

S1: Main Injector Protons to the Recycler
$T6 --> $2D --> $16 --> BES --> $\$S1_{MIBS}$ --> $\$S3_{MIBS}$
S2: Recycler Protons to the Main Injector
$T4 -->$\$S3_{RRBS}$ --> $2F
S3: Accumulator P-Bars to the Recycler
$T7 --> $9A --> $2D --> $\$7A_{MIBS}$ --> $\$S4_{MIBS}$
S4: Recycler P-Bars to the Main Injector
$T5 --> $2A --> $\$S4_{RRBS}$
(Multiple sequences of $T5 Recycler cycles and $2A Main Injector cycles are necessary to fill the Tevatron.)
S5: Tevatron P-Bars to the Recycler
$CE --> $T8 --> $T9 --> $T7 --> $2A --> $T10 --> $25 --> $\$S2_{MIBS}$ -->
$T11 --> $T12 --> $T13 --> $\$S4_{MIBS}$
(Multiple sequences of $T7 Recycler and $2A Main Injector cycles are necessary to empty the Tevatron of p-bars once the Tevatron is at 150 GeV.)

$\$S1_{RRBS}$: Initiate Proton Transfer from Recycler to Main Injector - This transfer event will be generated in a typical fashion by having a TCLK timer channel output sync up with the first available decoded $\$AA_{RRBS}$ event to form the $\$S3_{RRBS}$ event request. $T4 appears to be the natural reference. It could also process the output of a timer channel with a $2D reference with a state machine to form the appropriate event request.

$\$S3_{RRBS}$: Initiate Antiproton Transfer from Recycler to Main Injector - This transfer event will be generated by having a TCLK timer output sync up with the first available decoded $\$AA_{RRBS}$ event to form the $\$S4_{RRBS}$ event request. $T5 appears to be the natural reference though it may be too far away in time. It could also process the output of a timer channel with a $2A reference with a state machine to form the appropriate event request.

$\$S1_{MIBS}$: Initiate Beam Transfer from Booster to Main Injector - Generation of this event would require some state machine processing of the BES pulse from the Booster. For the general case, the occurrence of any Main Injector reset and the occurrence of any Booster reset except $17 would cause $\$S1_{MIBS}$ to be generated. It is necessary to have BES at MI-60, the location of the Main Injector RF system and the MIBS source, if the $\$S1_{MIBS}$ event is to be accurate. State processing of the $1F event might also serve as the event request for $\$S1_{MIBS}$. The possibility of timing the injection kicker at MI-10 with BES, as alternative to $\$S1_{MIBS}$, remains as a viable option.

$\$S2_{MIBS}$: Initiate Antiproton Transfer from Tevatron to Main Injector - Transfer cogging and diagnostic concerns again suggest this transfer event to be best placed on the MIBS rather than the TVBS clock. This event will be generated by having a TCLK timer channel output sync up with the first available decoded $\$AA_{MIBS}$ event to form the $\$S2_{MIBS}$ event request. New event $T10, which occurs when the Tevatron ramp has reached 150 GeV after the deceleration process, is likely the best reference for the timer channel. Some state machine processing of the actual event request signal is likely.

$\$S3_{MIBS}$: Initiate Proton Transfer from Main Injector to Recycler - This transfer event will be generated by having a TCLK timer channel output sync up with the first available decoded $\$AA_{MIBS}$ event to form the $\$S3_{MIBS}$ event request. $T6 appears to be the natural reference. It could also condition the output of a timer channel with a $2D reference with a state machine to form the appropriate event request.

$\$S4_{MIBS}$: Initiate Antiproton Transfer from Main Injector to Recycler - This transfer event is somewhat special in that two TCLK timer channels, one for each of the related S3 and S5 scenarios, are necessary to support event generation. The or'd timer channel outputs will sync up with the first available decoded $\$AA_{MIBS}$ event to form the $\$S4_{MIBS}$ event request. For the S3 scenario, either $T7 or $9A appear to be the natural reference for the first timer channel, the choice depending on their relative position in time. Some state machine processing is anticipated. For the S5 scenario, the aforementioned $T11 might serve as a reference for the second timer channel. One could also consider $T13 which occurs when the Main Injector ramp has reached 8 GeV after the deceleration process. As for the previous case, some state machine processing is probably required.

2.5. Vacuum Issues

Stainless steel beam tubes in which the vacuum is maintained with lumped ion-sputter pumps is the traditional technology used in the hadron accelerators at Fermilab. Though an aluminum alternative is under serious consideration, this report will discuss a stainless steel system in which innovations are applied to bring down the cost without invoking unreasonable technical risks. An important factor affecting the design of the system is the need for high reliability storage of the antiprotons. With the stated goal of surviving lightning strikes and power outages of up to an hour, manual sector valves and low outgassing rate beam tubes are required.

2.5.1. Beam Intensity Lifetime Requirement

The required beam intensity lifetime is determined by modeling the evolution of antiproton intensity in the Recycler assuming injections from the Tevatron and Accumulator. At the beginning of each collider cycle the Recycler contains the antiprotons recycled from the Tevatron. Every hour after the start of a collider store antiprotons stacked in the Accumulator are injected into the Recycler. It is assumed that the stacking rate is 20×10^{10} antiprotons/hour.

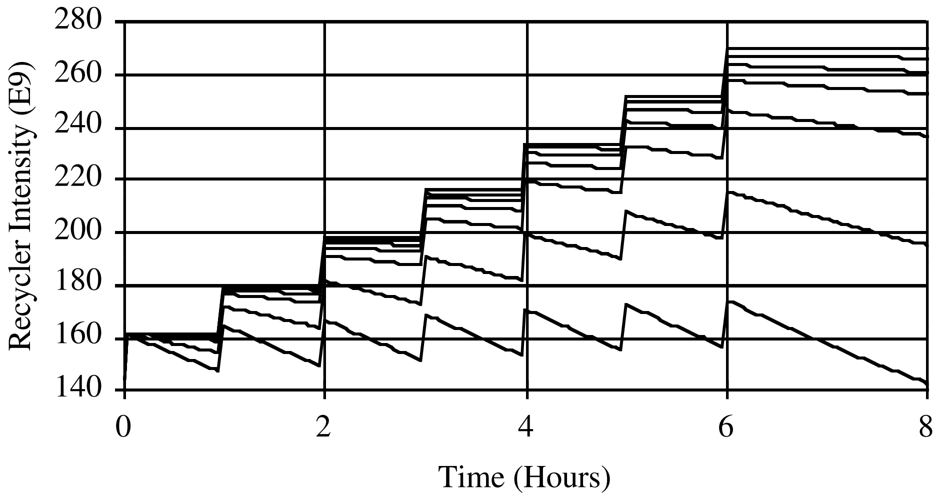

Figure 2.5.1: Assuming beam intensity lifetimes of infinity (top), 500, 200, 100, 50, 20, and 10 hours (bottom), evolution of the antiprotons injected from the Tevatron (recycled) and the Accumulator (stacked).

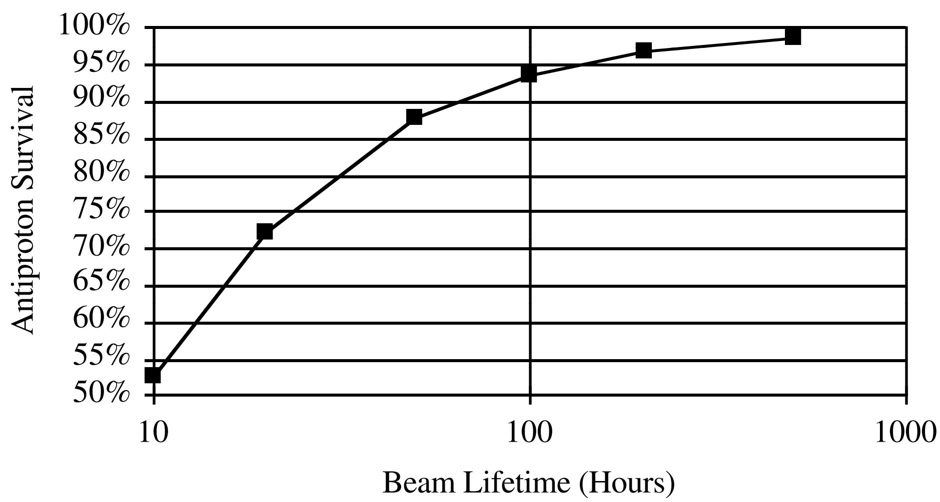

Figure 2.5.2: Fraction of the injected antiprotons (both recycled and stacked) which survive to the start of the next Tevatron Collider store.

The results of this model, for a range of beam intensity lifetimes, are displayed in figure 2.5.1. Note that using a criterion in which 95% survival is satisfactory over the 8 hours between the start of Tevatron Collider stores, it is evident that beam intensity lifetimes of 100 hours or greater are required in the Recycler. Integrating each of these curves, the percentage of recycled and stacked antiprotons available for luminosity generation in the next Tevatron Collider store can be calculated. The results of these integrations are shown in figure 2.5.2. Again, it is evident that a beam intensity lifetime of 100 hours or greater is necessary to support the antiproton storage mission of the Recycler.

2.5.2. Ion Trapping Requirement

The relativistic antiproton beam in the Recycler is composed of individual antiprotons which periodically collide with electrons circulating around residual atoms in the vacuum chamber. These electrons rebound away from the atoms with approximately 2 eV of kinetic energy [P. Zhou, Ph.D. thesis, 1993]. The momentum transfer to the ionized molecules is negligible. Because the ions are positively charged, they are attracted by the antiproton beam. In fact, because the ions are necessarily formed inside the transverse potential well of the antiproton beam, they will be trapped. Unless some mechanism is introduced to eliminate these trapped ions, the ion density will increase until it is equal to the beam density.

The rate at which the ion density increases R_i is determined by the equation [M. Reiser, "Theory and Design of Charged Particle Beams", pg. 273]

$$R_i = n_g \, n_b \, \sigma_i \, v \qquad , \quad (2.5.1)$$

where n_g is the gas density, n_b is the beam density, σ_i is the ionization cross-section, and v is the beam velocity. The standard relationship between the gas density and the partial pressure P of the gas in question is

$$n_g[m^{-3}] = 3.54 \text{x} 10^{22} \ P[\text{Torr}] \qquad . \quad (2.5.2)$$

The ionization cross-section depends on the velocity of the beam and the atomic properties of the gas in question. In the case of the Recycler the equation used to calculate the cross-section can be written in the approximate form

$$\sigma_i[m^2] = 1.9 \text{x} 10^{-24} \, A_1 \left\{ \text{Ln}\left(7.5 \text{x} 10^4 \, A_2 \, \gamma^2\right) - 1 \right\} \qquad , \quad (2.5.3)$$

The parameters A_1 and A_2 are molecule specific. The value of γ is 9.45 at a kinetic energy of 8.000 GeV. The results of calculations of ionization cross-section are listed in table 2.5.1.

Table 2.5.1: Values of the parameters A_1 and A_2 [M. Rudd, et. al., Rev. Mod. Phys. **57**, 965 (1985)] and the cross-sections themselves of relevant gasses in the Recycler vacuum system.

Gas	A_1	A_2	σ_i [m^2]
H_2	0.71	2.5	2.1×10^{-23}
N_2	3.8	0.52	1.0×10^{-22}
CO	3.7	0.54	1.0×10^{-22}

Assuming a peak Recycler antiproton intensity of 4×10^{12} in a circumference of 3.3 km, the peak longitudinal beam density λ_b is 1.2×10^9 antiprotons/m. The beam velocity is 3×10^8 m/s. Therefore, given assumptions justified later in this section for the vacuum partial pressures, the rate at which the longitudinal ion densities are growing can be calculated. The results of these calculations, and the estimation of the time it takes for the ion density to equal the beam density, are listed in table 2.5.2.

Table 2.5.2: Ion production rate calculations based on partial pressure predictions and an antiproton beam intensity of 4×10^{12}. The neutralization time of the beam for each gas does not assume the existence of the other gas.

Gas	Pressure [nTorr]	Gas Density [m^{-3}]	Ionization Rate [m^{-1} s^{-1}]	Neutralization Time [s]
H_2	0.1	3.5×10^{12}	2.6×10^7	46
$CO+N_2$	0.002	7.1×10^{10}	2.6×10^6	460

The average transverse rms beam size σ_r in the Recycler is 2.3 mm. Given a Gaussian transverse beam distribution and longitudinal density λ_b the beam density is described by the equation

$$n_b(r) = \frac{\lambda_b}{2\pi\,\sigma_r^2} \exp\left[-\frac{r^2}{2\sigma_r^2}\right] \quad . \qquad (2.5.4)$$

Therefore, the peak density at the beam center is 3.5×10^{13} antiprotons/m^3. If the beam has been neutralized to an ion density equal to the beam density, then using equation 2.5.2 we know that the effective peak pressure seen by the beam due to the trapped ion cloud is 3.5×10^{13} molecules/m^3, or a pressure of 1 nTorr. This calculation is an over estimate, since it ignores the fact that trapped ions can become multiply ionized, thereby neutralizing the space charge of the beam with fewer ions.

The pressure implication of the neutralized ion cloud around the antiproton beam will become evident later in the section. There are two other effects from these ions. First, a coherent instability can develop due to the electromagnetic coupling between the transverse oscillations of the antiprotons and those of the ions. Second, the ions will induce an incoherent tune spread due to the static transverse electrostatic field generated by the ion cloud.

The ion cloud has the same transverse dimensions as the beam, since the probability density of ionization has the same profile as the transverse beam density distribution. Therefore, equation 2.5.4 also describes the ion cloud density distribution. The radial electric field E_r generated by this distribution is

$$E_r(r) = \frac{e\lambda_b}{2\pi\,\varepsilon_o\, r}\left\{1 - \exp\left[-\frac{r^2}{2\sigma_r^2}\right]\right\} \quad , \quad (2.5.5)$$

where ε_o is the free space permittivity 8.854×10^{-12} F/m. The radial space charge force F_r is found by plugging equation 2.5.5 in the Lorentz equation to obtain

$$F_r(r) = \frac{e^2\lambda_b}{2\pi\,\varepsilon_o\, r}\left\{1 - \exp\left[-\frac{r^2}{2\sigma_r^2}\right]\right\} \quad . \quad (2.5.6)$$

At a radius small compared to the rms cloud radius this equation reduces to

$$F_r(r) = \frac{e^2\lambda_b}{4\pi\,\varepsilon_o\,\sigma_r^2}\, r \quad . \quad (2.5.7)$$

But this is the same force equation as found in either the horizontal or vertical plane of a quadrupole magnet. Converting this result into the form of a quadrupole gradient error ΔK yields the result

$$\Delta K = \frac{e^2\lambda_b}{4\pi\,\varepsilon_o\,\sigma_r^2}\,\frac{1}{P_o v} = \frac{r_o\,\lambda_b}{\left(\gamma\beta^2\right)\sigma_r^2} \quad , \quad (2.5.8)$$

where P_o is the antiproton beam momentum, r_o is the classical radius of the proton 1.53×10^{-18} m, and the quantities γ and β are the relativistic beam energy and velocity respectively (with the respective values of 9.45 and 0.9945). Plugging in all of the number expressed so far for the factors in the rhs form of equation 2.5.8 yields a space charge gradient of 3.7×10^{-5} m^{-2}.

The tune shift $\Delta\nu$ due to this gradient error is expressed as

$$\Delta\nu = \frac{1}{4\pi}\oint \beta(s)\,\Delta K\, ds \quad , \quad (2.5.9)$$

where the integral is evaluated around the circumference of the ring. Assuming a constant average beta function β_{ave} around the ring of 30 m, substituting equation 2.5.8 into equation 2.5.9 yields the result

$$\Delta\nu = \frac{r_o \lambda_b}{\left(\gamma\beta^2\right)\sigma_r^2} \frac{\beta_{ave} C}{4\pi} = \frac{3 r_o \lambda_b C}{2\pi\beta\, \varepsilon_N} \quad , \quad (2.5.10)$$

where C is the circumference of the ring and ε_N is the normalized 95% emittance. The value of the peak tune shift at the antiproton beam intensity of 4×10^{12} and full neutralization is 0.29, a value which is approximately two orders of magnitude too large for a stored beam. Therefore, it is imperative to employ methods for eliminating ions from the beam.

Three methods are planned for the Recycler. The first is the use of a coherent transverse beam closed orbit oscillation at the resonant frequency of the ion oscillation about the beam centroid. The transverse dampers installed in the Recycler to combat coherent instabilities are planned to have electronics capable of exciting this closed orbit oscillation, just as in the Accumulator. The second is to maintain a gap in the longitudinal beam distribution to destabilize the ions. This requires the constant use of a set of barrier bucket pulses to maintain an empty section of beam azimuth. The third is to employ clearing electrodes to sweep away ions from the beam potential well. In the Recycler there are two beam position monitors in each half cell which will be used as clearing electrodes.

2.5.3. Ion Clearing with a Longitudinal Gap in the Beam

Maintaining a gap in the beam distribution destabilizes low mass ions due to the fact that the time periodicity of the instantaneous beam current has the same effect on the ions as if the ions were circulating in a circular accelerator experiencing a comparable lattice. Assume that the beam is not neutralized, and that the ions have thermal kinetic energies. Then only the electric field from the beam has a significant impact on the ion motion. Equation 2.5.7 describes the radial force due to electric field of the antiproton beam. Since this force is attractive, an ion of mass M undergoes a radial oscillation about the beam centroid described by the differential equation

$$\ddot{z} + \frac{e^2 \lambda_b}{4\pi\, \varepsilon_o\, \sigma_r^2\, M} z = 0 \quad . \quad (2.5.10)$$

Let ω_i be the ion angular frequency indicated in this harmonic oscillator equation. At the antiproton intensity of 4×10^{12} molecular hydrogen H_2 has a ion angular frequency of 4×10^6 rad/s. At this rate the small amplitude H_2 ion undergoes 7.13 transverse oscillations for every one antiproton revolution around the Recycler. If T_b is the length of the beam distribution and T_g is the length of the gap, then the matrix equation describing the one-turn map of the ion coordinates (z,v) is

$$\begin{pmatrix} z \\ v \end{pmatrix}_{n+1} = \begin{pmatrix} \cos(\omega_i T_b) & \frac{1}{\omega_i}\sin(\omega_i T_b) \\ -\omega_i \sin(\omega_i T_b) & \cos(\omega_i T_b) \end{pmatrix} \begin{pmatrix} 1 & T_g \\ 0 & 1 \end{pmatrix} \begin{pmatrix} z \\ v \end{pmatrix}_n \quad . \quad (2.5.11)$$

The stability of the ions is determined by the condition that the trace of the one-turn matrix

$$\begin{pmatrix} \cos(\omega_i T_b) & T_g \cos(\omega_i T_b) + \frac{1}{\omega_i}\sin(\omega_i T_b) \\ -\omega_i \sin(\omega_i T_b) & \cos(\omega_i T_b) - \omega_i T_g \sin(\omega_i T_b) \end{pmatrix} \tag{2.5.12}$$

be

$$\left|\cos(\omega_i T_b) - \tfrac{1}{2}\omega_i T_g \sin(\omega_i T_b)\right| \le 1 \quad . \tag{2.5.13}$$

Let $A = \omega_i T_g/2$ and $\phi = \omega_i T_b$. The magnitude of this equation for various choices of A over the full 2π range of ϕ is shown in figure 2.5.3. Note that the ion motion is unstable when the curve is greater than unity. Since ϕ depends critically on the precise beam intensity, it is very hard to control accurately enough to always guarantee that the it is in a region of instability. On the other hand, for values of A of approximately 5 or greater, the ion is generally unstable independent on the detailed beam intensity.

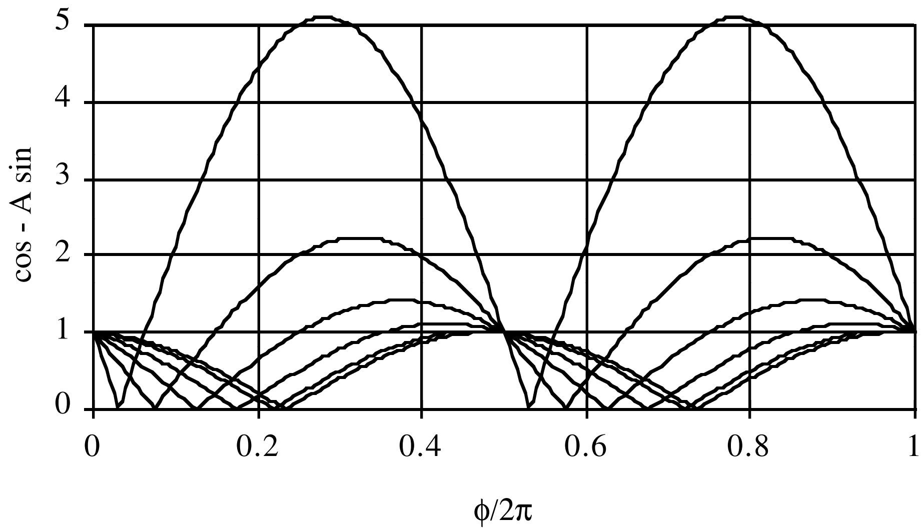

Figure 2.5.3: Map of equation 2.5.13 for various choices of the defined parameter A over the full 2π range of ϕ. The values for A are 5 (top), 2, 1, 0.5, 0.2, and 0.1 (bottom).

For the case again of molecular hydrogen H_2, the value of A for a 2 μsec long ion clearing gap is 5. For the minimum operational current when only the recycled beam is in the accelerator A drops to 2 for the same size clearing gap. As will be seen in the sections on intrabeam scattering and stochastic cooling, it is desirable to compress the beam longitudinally as much as possible, to at most half of the Recycler circumference. Under these conditions with only recycled antiprotons the factor A is again greater than 11. For stacking from an empty Recycler, assuming transfers of intensities greater than or equal to 2x1011 antiprotons, if the 1.6 μsec beam pulse length from the Accumulator is maintained with barrier buckets the minimum value for A is greater than 6. On the other hand, with an atomic number of 28, either CO or N_2 are almost always expected to be stable in the presence of the ion clearing gap.

For unstable ions the growth rate of their oscillation amplitudes about the beam is

$$\tau = \frac{T_o}{\cosh^{-1}\left(\left|\cos(\omega_i T_b) - \frac{1}{2}\omega_i T_g \sin(\omega_i T_b)\right|\right)} \quad , \quad (2.5.14)$$

where T_o is the revolution period of the antiprotons in the Recycler. For values of A and f where the beam motion is unstable the value of the growth rate is calculated and plotted in figure 2.5.4. Note that the for most of the phase space the growth time is approximately equal to the revolution period.

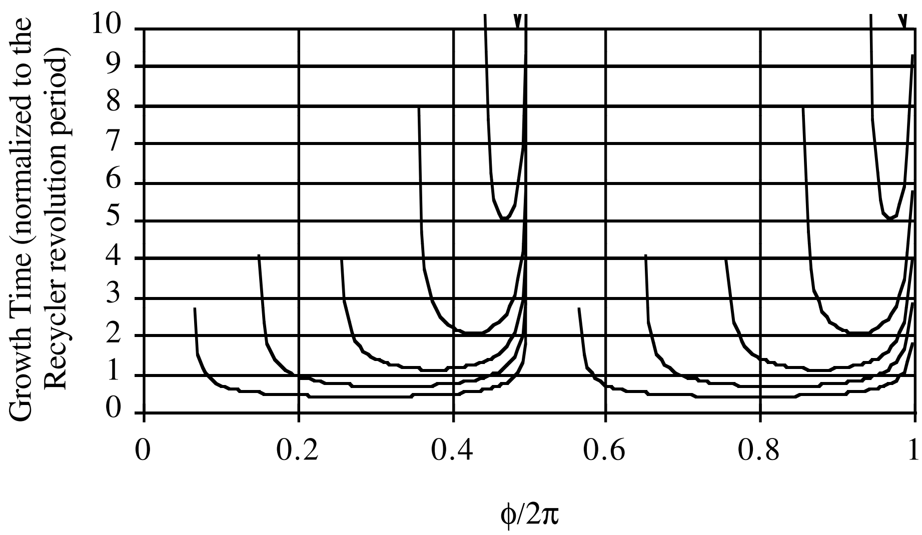

Figure 2.5.4: Map of equation 2.5.14 when the beam motion is unstable. The values for A are 5 (bottom), 2, 1, 0.5, 0.2, and 0.1 (top).

If it is assumed that the ion amplitude growth time is also the characteristic time it takes for the ion to be cleared from the beam, then the equilibrium ion longitudinal density λ_i is described by the equation

$$\lambda_i = R_i \tau \quad . \quad (2.5.15)$$

For the case of $\tau = T_o$ and the value of R_i for H_2 listed in table 2.5.2, the equilibrium ion longitudinal density is 291 H_2 ions/m! It should be pointed out that larger amplitude ions see a net field which is different from that assumed in the above linearized theory. In the cases of marginal growth linearized growth rates the net reduction in focusing experienced by the ions may slow down or even halt their escape from the beam.

2.5.4. Ion Clearing with Clearing Electrodes

In the case of H_2 where ϕ and A do not lead to unstable oscillations around the antiproton beam, and for the case of CO and N_2 in general, another method of ion clearing is required. This is the purpose of the clearing electrodes. A pair of clearing electrodes on opposite sides of the vacuum chamber with opposite voltage generate a transverse electric field. When that electric field is greater than the maximum radial electric field generated by the beam, any ions between the electrodes are stripped away from the beam.

The electric field generated by the beam is described by equation 2.5.5. Taking the derivative of the electric field with respect to radius and setting the result equal to zero, the radius at which the electric field is maximum is calculated to be

$$r_{max} = 1.585\,\sigma_r \quad . \qquad (2.5.16)$$

Substituting this result into the electric field equation yields the result

$$E_{max} = \frac{0.45 e\,\lambda_b}{2\pi\varepsilon_o\,\sigma_r} \quad . \qquad (2.5.17)$$

With an antiproton intensity of $4x10^{12}$ in the Recycler, the maximum radial electric field is found to be 675 V/m. The largest effective separation d of the clearing electrodes across the vacuum chamber is 9.5 cm. The minimum voltage across the electrodes is related to this separation and the maximum radial electric field according to

$$V_{min} = E_{max}\,d \quad . \qquad (2.5.18)$$

Plugging in the above number, the minimum voltage per electrode is approximately 32 V.

The ions are traveling with kinetic energies determined by their temperature, which is equal to room temperature 300°K. Table 2.5.3 contains a summary of the ion velocities, and for future reference when ion propagation in the gradient magnets are discussed their cyclotron orbit in a 1.5 kG magnetic field.

Table 2.5.3: RMS thermal ion velocity and rms cyclotron orbit radius as a function of gas species assuming room temperature. The cyclotron orbit radius assumes the 1.5 kG magnetic field in the Recycler gradient magnets. The overvoltage is the amount of additional voltage required to accelerate an rms ion into the negative electrode, thereby eliminating the ion from the beam.

Gas	Atomic Mass	rms Velocity [m/s]	rms Cyclotron Radius [mm]	Overvoltage [V]
H_2	2	1113	0.15	0.0013
$CO+N_2$	28	297	0.58	0.0013

In order to assure that the ions leave the beam while they ballistically traverse the clearing electrodes, an additional accelerating voltage greater than the above 32 V is necessary. The electrodes are 1' long. Assume that a particle traveling at the rms velocity straight down the center of the vacuum chamber must be deflected enough to strike the negative electrode. The additional voltage required per electrode for each species of gas to perform this task is listed in the right most column of table 2.5.3. It is truly negligible.

Table 2.5.4: Mean free path calculation assuming the effective molecular diameter to be $2x10^{-10}$ m. The point of this calculation is to verify that the ion motion in the beam is ballistic in nature, since the mean free path is much longer than the vacuum chamber and the distance between clearing electrodes.

Gas	Pressure [nTorr]	Gas Density [m^{-3}]	Mean Free Path [m]
H_2	0.1	$3.5x10^{12}$	$2.3x10^6$
$CO+N_2$	0.002	$7.1x10^{10}$	$1.1x10^8$

As shown in table 2.5.4, the motion of ions is not significantly affected by other ions in the range of pressure that is found in the Recycler vacuum system. Therefore, it is not unreasonable to assume that a molecule ionized in the beam will travel unmolested longitudinally with an rms speed listed in table 2.5.3. This geometry, with the approximate relative geometry between two clearing stations in a Recycler half cell, is shown in figure 2.5.5.

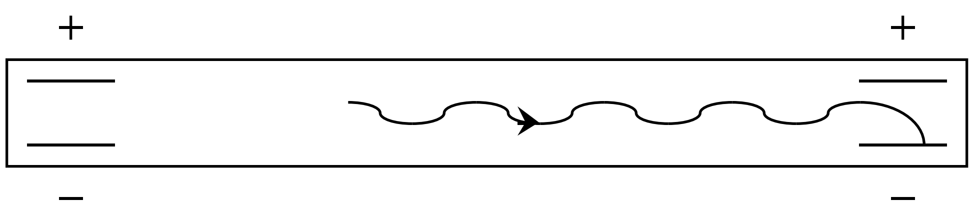

Figure 2.5.5: Sketch of an ionized molecule with an initial longitudinal velocity in a geometry very similar to that inside a Recycler half cell.

The clearing electrodes act as a black hole, eliminating every ion that traverses them. If the distance between the clearing electrodes is L_{ce}, and the rms velocity of an ion is σ_v, then the average time τ it takes an ion heading toward a particular electrode to be eliminated from the beam is

$$\tau = \frac{L_{ce}}{\sigma_v} \quad . \quad (2.5.19)$$

Plugging this result into equation 2.5.15 yields an estimate of the equilibrium average trapped ion density between the clearing electrodes. Using previously present values for the relevant parameters, the calculations this average ion density for each gas species is listed in table 2.5.5. The worst case density is 10,000x lower than expected at neutralization.

Table 2.5.5: Calculation of the equilibrium ion longitudinal density assuming a distance between clearing stations of 6 m.

Gas	Clearing Time [ms]	Ion Density [m^{-1}]
H_2	5.3	1.4×10^5
$CO+N_2$	20	5.2×10^4

The Recycler vacuum system also has gradient magnets. When a gas molecule is ionized inside the magnet, the ions do not simply propagate out at their thermal velocities. As shown in table 2.5.3, the ions execute very tight horizontal cyclotron oscillations around the magnetic field lines. If these magnets were pure dipoles, the only mechanism for ion transport to the clearing electrodes would have been ExB drift generated by the space charge radial electric field of the beam. At the radial field maximum of 675 V/m, for a relatively improbable ion more than a sigma away from the beam center, the drift velocity is 675 / 0.15= 4500 m/s. But the small amplitude ions see an order of magnitude smaller electric field, and for the case of low beam intensity the electric field is yet again another order of magnitude smaller. On the other hand, that still leaves a factor of 100x lower density than expected if the beam were completely neutralized. But this is the factor of 100x that was needed to reduce the tune spread effects of the ion cloud to manageable levels.

In addition, the gradient portion of the Recycler bend magnets introduce ∇B drift. As an ion executes horizontal cyclotron orbits, the gradient in the dipole field causes these orbits to have a horizontal position dependent radius of curvature. This causes the particle to drift longitudinally. The drift velocity v_d depends on the cyclotron radius r_c, the field gradient g, and the cyclotron frequency f_c according to the equation

$$v_d = \pi f_c \, g \, r_c^2 \quad . \quad (2.5.20)$$

Table 2.5.6 contains the results of this calculation for the gas species of interest. The gradient for the normal cell Recycler gradient magnets is 2.5 m^{-1}. Note that compared to the neutralizing ion density of 1.2×10^9 m^{-1}, the H_2 density in the magnet is almost unaffected whereas the $CO+N_2$ density is a factor of 20x below neutralization. Taking into account the fact that the gradient magnets make up approximately half of the ring, this indicates that with clearing electrodes only that $CO+N_2$ neutralization can be avoided. The combination of a gap and electrodes seems to be needed for H_2.

Table 2.5.6: Calculation of the equilibrium ion longitudinal density in a gradient magnet assuming ∇B drift as the mechanism for trapped ion loss. The expected average equilibrium ion densities in the magnets are also calculated.

Gas	Cyclotron Freq. [MHz]	Drift Speed [m/s]	Magnet Ion Density [m^{-1}]
H_2	1.1	0.19	5.2×10^8
$CO+N_2$	0.082	0.22	5.2×10^7

2.5.5 Vacuum Specification

The beam tube vacuum pressure requirement is determined by antiproton intensity lifetime, antiproton emittance growth, and ion trapping considerations. The emittance growth rates should be small compared to the anticipated intrabeam scattering growth rates. The intensity lifetime should be long enough insure that the stacking rate necessary to achieve the required antiproton intensity is not increased by more than a few percent. Because vacuum pressures always improve with time, the specification quoted in this section will apply to the initial pressure needed for reasonable operations.

The transverse normalized 95% emittance growth rate is determined by multiple Coulomb scattering with the nuclei of the residual gas in the beam tube. Assuming a relativistic beam, the equation describing this growth rate can be written as

$$\dot{\varepsilon}_n = \frac{3\langle\beta\rangle}{\gamma_r}\left(\frac{15\ \mathrm{MeV}}{mc^2}\right)^2 \frac{c}{L_{rad}} \quad , \quad (2.5.21)$$

where <β> is the average beta function of the accelerator, γ_r is the relativistic energy of the beam, and L_{rad} is the radiation length of the gas at a given temperature and pressure. Radiation length values at standard temperature (0 °C) and pressure (760 Torr) are listed in table 2.5.7.

Table 2.5.7: Radiation lengths for the two constituent molecules commonly found in a high vacuum stainless steel system such as that expected for the Recycler ring.

Gas	Radiation Length (g/cm^2)	Density @STP (g/l)	Radiation Length (m)
H_2	61	0.090	6800
$CO+N_2$	38	1.25	300

Table 2.5.8: Normalized 95% emittance growth rate for each component gas in a high vacuum system assuming a total pressure of approximately 1 nTorr and a standard ratio of 5:1 between hydrogen and nitrogen/carbon monoxide.

Gas	Partial Pressure (nTorr)	Radiation Length (m)	Emittance Growth Rate (π mmmr/hr)	Emittance Growth Time (hrs)
H_2	0.1	5.2×10^{16}	0.05	200
$CO+N_2$	0.002	6.0×10^{15}	0.05	200

Assuming an average beta function value of 30 m and a kinetic energy of 8 GeV, the emittance growth rates for the same constituent vacuum gasses are listed in table 2.5.8. Note that the measured and expected ratio of hydrogen to nitrogen/carbon monoxide is set at 50:1. As will be shown later, these pressures are the result of measured outgassing rates and calculated pumping speeds. In order to calculate an emittance growth time, a base emittance of 10 π mmmr is assumed.

The stochastic cooling system is anticipated to have an emittance cooling time of approximately 4 hours. From table 2.5.8 it is can be shown that maintaining an average $CO+N_2$ partial pressure of less than 0.1 nTorr is necessary for Recycler operations.

Table 2.5.9: Nuclear interaction lengths for the two constituent molecules commonly found in a high vacuum stainless steel system.

Gas	Nuclear Int. Length (g/cm^2)	Density @STP (g/l)	Nuclear Interaction Length (m)
H_2	51	0.090	5700
$CO+N_2$	88	1.25	704

Table 2.5.10: Intensity lifetime due to nuclear interactions with each component gas in a high vacuum system.

Gas	Partial Pressure (nTorr)	Nuclear Interaction Length (m)	Antiproton Loss Time (hrs)	Antiproton Loss Rate (10^{10}/hrs)
H_2	0.1	$4.3x10^{16}$	40,000	0.0063
$CO+N_2$	0.002	$1.4x10^{17}$	250,000	0.0010

The other consideration is particle lifetime. The two mechanisms which remove particles from the ring are nuclear interactions and large angle Coulomb scattering (Rutherford scattering). Nuclear interactions are typically broken down between elastic and inelastic scattering. Though a portion of the elastically scattered particles would stay in the accelerator, it is easier to take the worst case assumption that they are all lost. In that case the total cross-sections, characterized as a nuclear interaction length, is used. Table 2.5.9 contains the nuclear interaction lengths for the expected constituent gasses in the vacuum tube. In table 2.5.10 the lifetime and particle loss rates are calculated using a base intensity of $250x10^{10}$ antiprotons in the Recycler.

Single large angle Coulomb scattering angles greater than the angular acceptance of the Recycler occur with a frequency described by the equation

$$\sigma_{el} = \frac{2\pi r_p^2 Z^2}{\gamma_r^2} \frac{\beta_y}{A_y} \quad . \quad (2.5.22)$$

The lifetime associated with this cross-section is

$$\tau_{el} = \frac{1}{n_{gas}\, \sigma_{el}\, \beta c} \quad , \quad (2.5.23)$$

and r_p=$1.535x10^{-18}$ m. The results of these calculations are listed in table 2.5.11.

Table 2.5.11: Intensity lifetime due to large angle Coulomb scattering.

Gas	Partial Pressure (nTorr)	Cross-Section (mbarns)	Antiproton Loss Time (hrs)	Antiproton Loss Rate (10^{10}/hrs)
H_2	0.1	17	30,000	0.008
$CO+N_2$	0.002	870	30,000	0.008

In conclusion, even though its partial pressure is lower than the hydrogen, the $CO+N_2$ is comparable in both the particle loss and the emittance growth rate. A partial pressure less than 1×10^{-10} Torr is desirable for those species.

2.5.6. Outgassing of Stainless Steel

The spacing and pumping speed of the lumped ion-sputter and titanium sublimation pumps in a traditional Fermilab system is determined by the outgassing rate of gas molecules from the surface of the stainless steel vacuum tube. Because the cost of the vacuum system scales with the number of pumps, minimizing this outgassing rate is very desirable.

Upon chemically cleaning a stainless steel tube and performing a 150°C bake after system assembly, a hydrogen surface outgassing rate of 1×10^{-12} T-l/cm^2-sec is achievable. At this point the only other gas in the system is $CO+N_2$, which comes dominantly from the ion pumps and ion gauges. The hydrogen comes from diffusion of molecules out of the bulk of the stainless steel material. The key to reducing the cost of the Recycler vacuum system is to eliminate this bulk hydrogen.

High concentrations of hydrogen exist in stainless steel because of one step in it's production, when the steel is quenched in a hydrogen atmosphere. It has been found [R. Calder and G. Lewin, Brit. J. Appl. Phys. **18**, 1459 (1967)] that the hydrogen can be removed by heating the stainless steel in a good vacuum ($<10^{-6}$ Torr) at a temperature of approximately 500°C. Using this technique, measurement results at Fermilab with a 30 m test vacuum system have found surface outgassing rates of 2×10^{-13} T-l/cm^2-sec, even though it turns out that the ultimate pressure during the bake was only 10^{-3} Torr and multiple vacuum accidents during studies. More details concerning the hydrogen degassing oven and its operation can be found in chapter 3.

The calculation of time and temperature vs. hydrogen degassing of stainless steel is rather straightforward. Assume that an infinite slab of stainless steel of thickness d is placed in a perfect vacuum and heated to some temperature T. The one dimensional diffusion equation describing this situation is

$$D\frac{\partial^2 c}{\partial x^2} = \frac{\partial c}{\partial t} \quad . \qquad (2.5.25)$$

The diffusion coefficient D as a function of some typical outgassing temperatures is plotted in figure 2.5.6. The initial condition is that the stainless steel is uniformly saturated with hydrogen at some initial concentration c_o. As compared to an atmospheric hydrogen concentration of 1.4×10^{-4} T-l/cm^3, the initial concentration found in 300 series austentic stainless steels is 0.3 T-l/cm^3. Outside of the slab it is assumed that a perfect vacuum exists. The solution of the differential equation with these boundary conditions can be written in terms of an infinite sum

$$c(x,t) = c_o \frac{4}{\pi} \sum_{n=0}^{\infty} \frac{1}{(2n+1)} \sin \frac{\pi(2n+1)x}{d} \exp\left[-\left(\frac{\pi(2n+1)}{d} \right)^2 Dt \right] \quad . \quad (2.5.26)$$

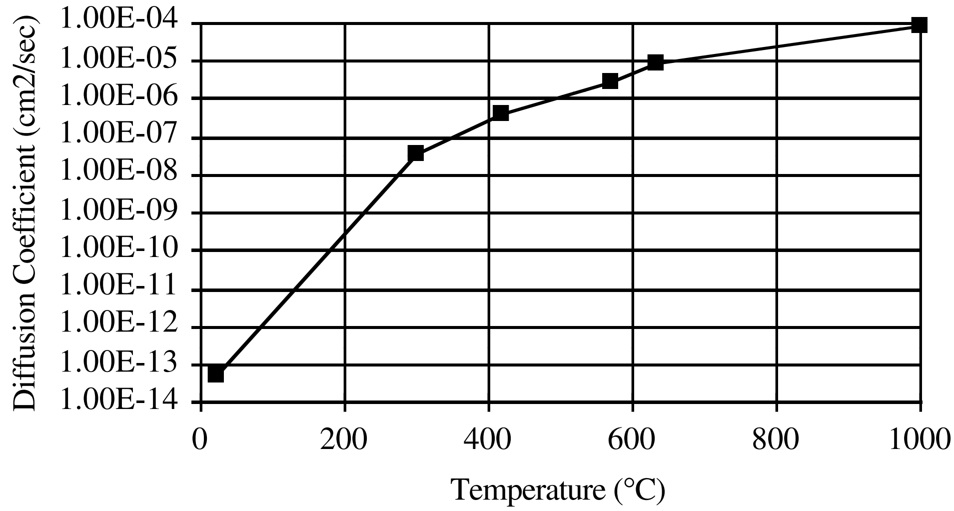

Figure 2.5.6: Hydrogen diffusion rate as a function of temperature in stainless steel. The data points are at typical degassing temperatures. The lines are for the purpose of interpolation.

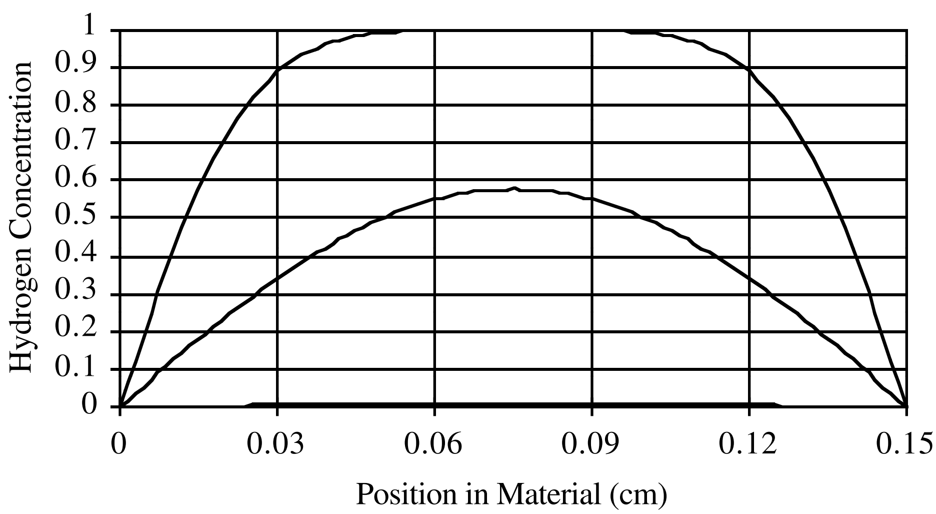

Figure 2.5.7: Hydrogen concentration profile across the beam tube wall as a function of time at 500°C. In the beginning the concentration is uniform and scaled to unity. The curves show the concentration profiles after 60 sec, 10 minutes, and 1 hour. After 3 hours the concentration is 1x10^{-7}.

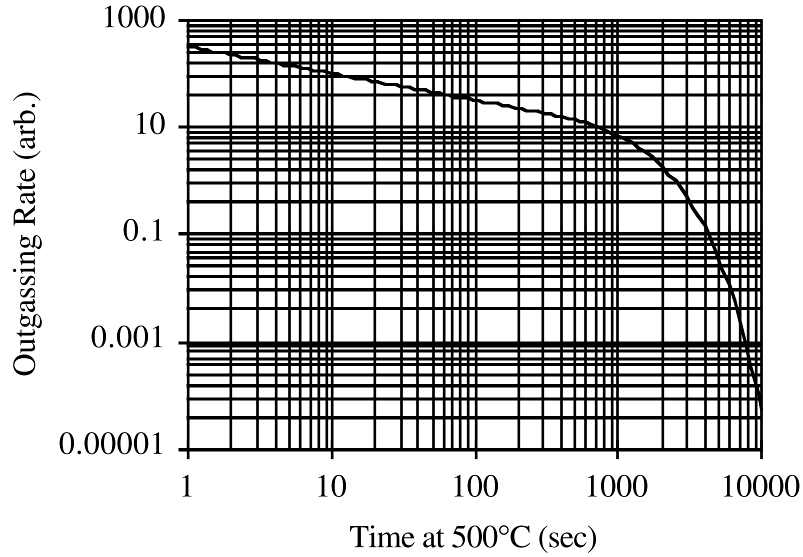

Figure 2.5.8: Hydrogen outgassing rate after cooldown as a function of the time spent at 500°C for degassing.

For the case of Recycler vacuum chamber, using a diffusion coefficient of 1×10^{-6} cm^2/sec (500°C) and a thickness d of 0.065" (approximately 1.5 mm), the concentration profile through the vacuum tube wall as a function of position in the wall and time at temperature is plotted in figure 2.5.7.

The surface outgassing rate σ_q of hydrogen from either surface is simply the derivative of the hydrogen concentration at the surface times the diffusion coefficient

$$\sigma_q(t) = D\left(\frac{\partial c}{\partial x}\right)_{x=0} = \frac{4c_o D}{d}\sum_{n=0}^{\infty}\exp\left[-\left(\frac{\pi(2n+1)}{d}\right)^2 D\,t\right] \quad . \quad (2.5.27)$$

Figure 2.5.8 contains a plot of the surface outgassing rate after cooldown as a function of time the vacuum tube was degassed at 500°C. The plan is to bake the tubes at 500°C for 6 hours with an oven pressure less than 1×10^{-6} Torr to guarantee full degassing.

2.5.7. Pressure Calculations

The pressure P(z) at some azimuth z around the ring is calculated using the differential equation

$$c\frac{d^2P}{dz^2} - s\,P = -q \quad , \quad (2.5.28)$$

where c(z) is the specific conductance of the vacuum tube, s(z) is the linear pumping speed, and q(z) is the specific outgassing rate. If these coefficients of the differential equation are piecewise constant, then the solution in any section of vacuum tube is

$$P(z) = A\exp\left[\sqrt{\frac{s}{c}}\,z\right] + B\exp\left[-\sqrt{\frac{s}{c}}\,z\right] + \frac{q}{s} \qquad . \quad (2.5.29)$$

Just as in the case of dispersion function lattice calculations, this solution lends itself to matrix calculations on the basis vector (P,Q,1), where Q(z) is the flow rate of gas down the tube at the azimuth z.

In a lumped stainless steel system the pumps and beam tubes are treated as separable (similar to the concept of separated function magnets). Therefore, in a vacuum tube the pumping speed is zero. The specific conductance of the elliptical cross-section beam tube can be written as

$$c[m-l/s] = 1.30\frac{(a[cm]\,b[cm])^2}{\sqrt{a^2+b^2}}\sqrt{\left(\frac{T[^\circ K]}{300}\right)\left(\frac{28}{M}\right)} \qquad , \quad (2.5.30)$$

where a and b are the half width and half height of the inside surface of the vacuum tube, T is the temperature of the system, and M is the atomic mass of the gas molecules (the equation is referenced to room temperature and the atomic mass of nitrogen).

Table 2.5.12: Parameters expected to describe the vacuum system in the Recycler ring. This spacing corresponds to three 30 liter/sec pump (either ion or titanium sublimation) per half cell, where the pumping speed (assuming ion pumps) was derated to account for saturation and low pressures at the pump.

Parameter	H_2	CO/N_2
Lumped Pump Pumping Speed (L/s)	30	10
Surface Outgassing Rate (T-L/s-cm^2)	$2x10^{-13}$	$1x10^{-15}$
Distance between Lumped Pumps (m)	5.75	5.75
Total Width of Elliptical Pipe (inch)	3.75	3.75
Total Height of Elliptical Pipe (inch)	1.75	1.75
Molecular Mass of the Gas	2	28
Specific Conductance (m-L/s)	100	28
Specific Outgassing Rate (T-L/s-m)	$4.4x10^{-10}$	$2.2x10^{-12}$
Pressure at Lumped Pumps (nTorr)	0.084	0.0013
Pressure Halfway between Pumps (nTorr)	0.100	0.0016
Average Pressure (nTorr)	0.096	0.015

To convert from the surface outgassing rate σ_q to the specific outgassing rate q it is necessary to multiply σ_q by the surface area per unit length. For an elliptical beam pipe

$$q[T-l/s-m] = 100\pi\sqrt{2(a[cm]^2+b[cm]^2)}\;\sigma_q[T-l/s-cm^2] \qquad . \quad (2.5.31)$$

Table 2.5.12 contains an example of typical parameter values used for calculating the Recycler vacuum performance. The ion pumps to be used are 30 liter/sec pumps, but the actual pumping speeds are derated because of the low pressures and assuming that the pumps are nitrogen saturated during pumpdown. The majority of the pumps are of the titanium sublimation variety, which have much lower ultimate pressure and much higher typical pumping speeds. The present titanium sublimation pumps are also planned to have a speed of 30 liter/sec. Figures 2.5.9 and 2.5.10 show the dependence of pressure on position in the beam tube. Note that the average pressures described are much lower than assumed in the lifetime discussions above.

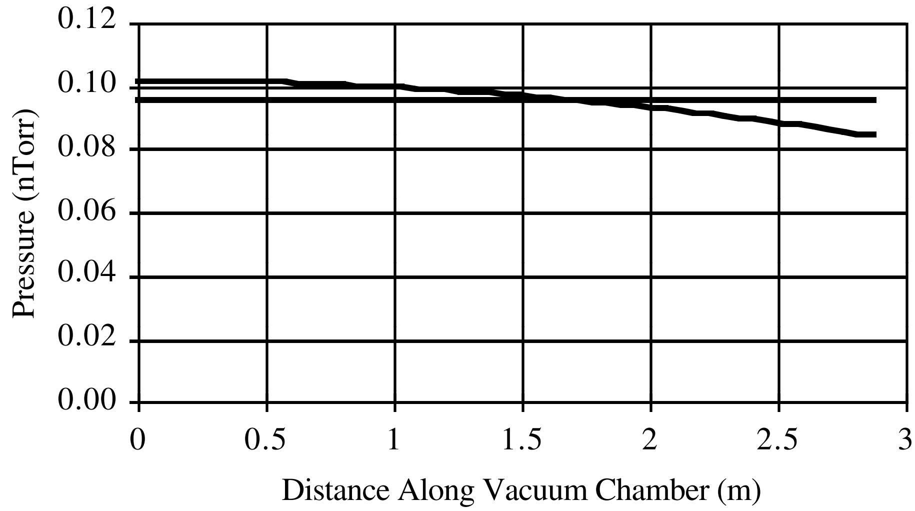

Figure 2.5.9: Hydrogen partial pressure as a function of distance along the vacuum tube. The origin is the symmetry point halfway between any two pumps. The parameters which generated this figure are listed in table 2.5.12. The horizontal line designates the average pressure.

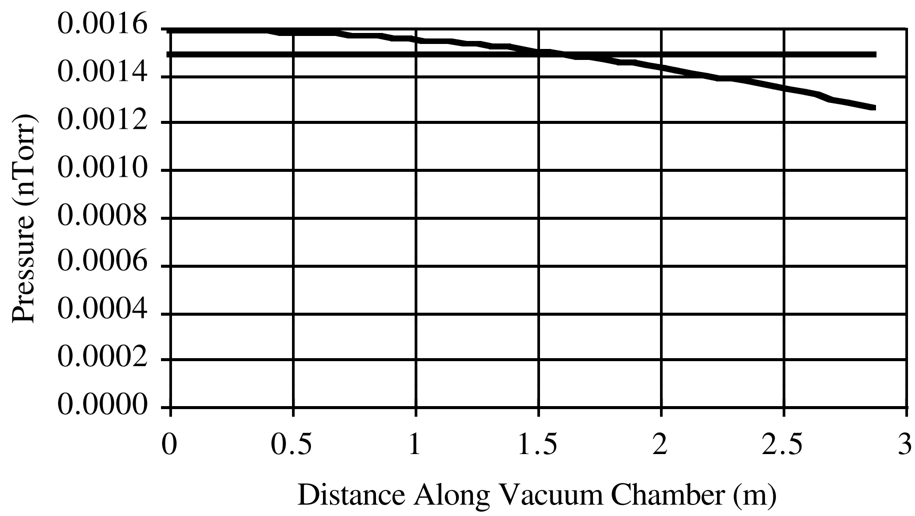

Figure 2.5.10: $CO+N_2$ partial pressure as a function of distance along the vacuum tube. The origin is the symmetry point halfway between any two pumps. The parameters which generated this figure are listed in table 2.5.12. The horizontal line designates the average pressure.

2.5.8. Magnetic Shielding

There are many sources of time-dependent magnetic fields which if left unshielded would modulate the closed orbit position and tune of the Recycler beam. Therefore, it has been decided to generate a hermetic seal of magnetic shielding around the Recycler vacuum chamber. In order to save money the insitu bake insulation and the magnetic shielding have been merged into the same effort. Because of this link to the insitu insulation, and because of the need to integrate the shielding with the vacuum fabrication, magnetic shielding is one of the responsibilities of the vacuum Recycler group. A sketch of the geometry of the magnetic shielding and insitu bake insulation is displayed in figure 2.5.11. The regions of vacuum chamber occupied by magnets do not require shielding due to the thick flux return they employ.

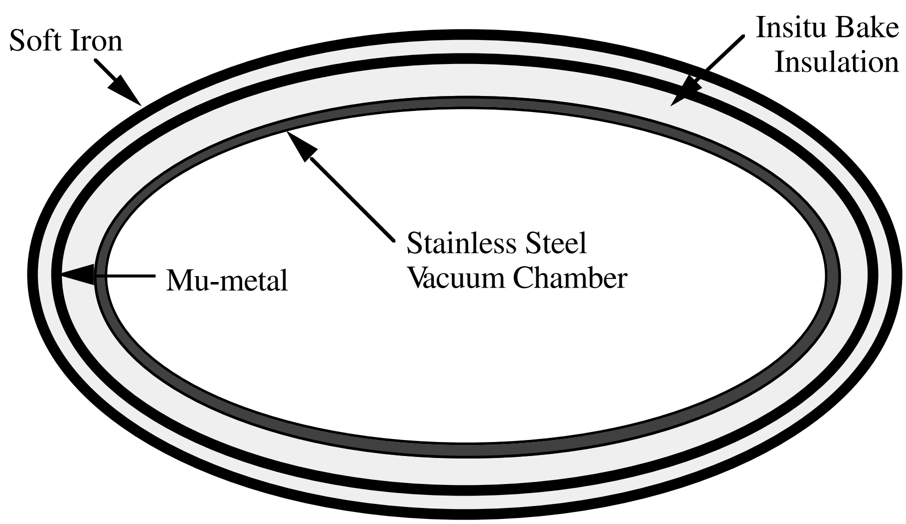

Figure 2.5.11: Sketch of the integrated magnetic shielding and insitu bake insulation for the Recycler ring.

.

The dominant sources of stray time-dependent magnetic fields at the Recycler tunnel position are:

1) Main Injector magnet fringe fields. These have been measured to be no more than 2 Gauss at the Recycler position [A. Mokhtarani & P. Mantsch, MTF-94-0052 (1994)].
2) Main Injector magnet bus bypasses. By calculating the dipole field generated by a pair of busses near the wall at the Main Injector elevation, a maximum field of 2 Gauss is calculated.
3) Uncompensated quadrupole loop current. The focusing and defocusing quadrupole circuits are each single loops around the tunnel. Therefore, the net current difference between these loops will generate a net magnetic flux through the wetland inside the Main Injector. More important, it would generate approximately 4 Gauss at the Recycler beam pipe.

4) High current cables in trays. One example would be Lambertson cables. Estimates generate fields as high as 5 Gauss.

In order to firm up these estimates and to identify any unanticipated source of field, a flux measurement experiment is being designed for the Main Ring tunnel at the comparable elevation of the Recycler. Another purpose of this test is to measure the actual field attenuation one obtains from magnetic shielding. There is some doubt as the validity of more detailed calculations of magnetic shields in the milliGauss field range. It is because of these doubts that only semi-quantitative calculations are presented below.

A system capable of shielding the beam to an extent comparable to the dipole field strength criterion is necessary. The fields in the gradient magnets is specified to have a maximum allowable error of 5×10^{-4} in a field of 1.5 kG. This corresponds to approximately 1 Gauss over roughly 4 m. In order to assure that systematic or random effects from the time dependent fields are negligible, especially in alignment sensitive regions such as the stochastic cooling pickups, a stray field goal at the Recycler beam of 10 mG has been specified.

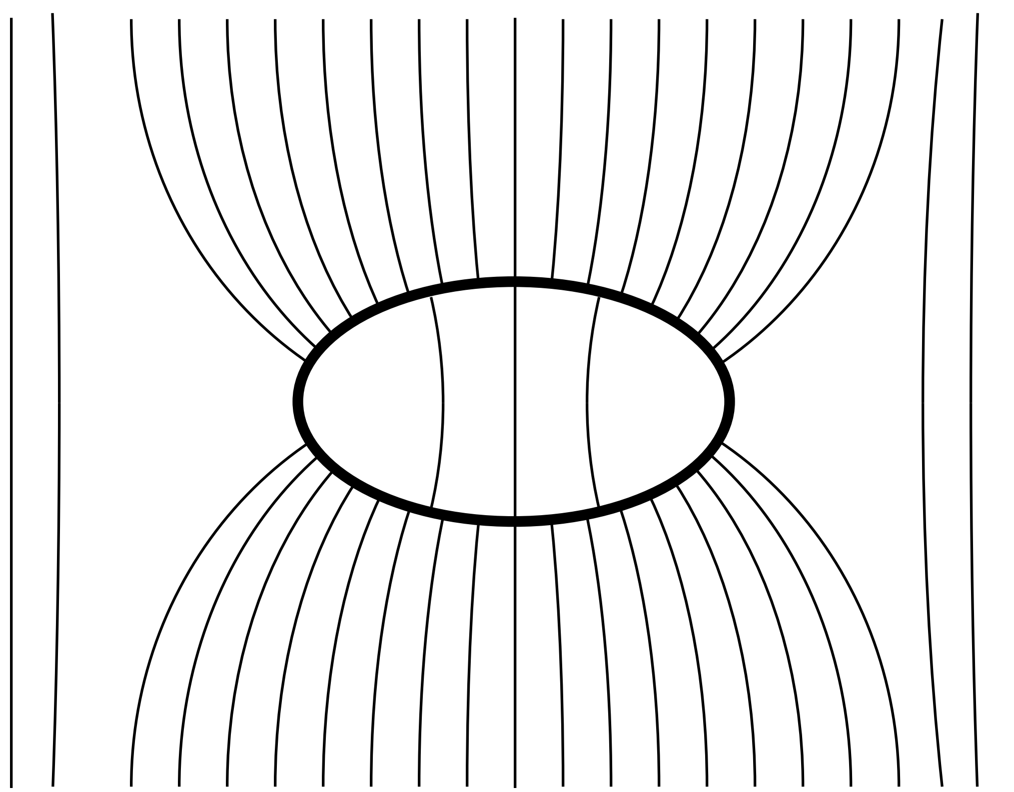

Figure 2.5.12: Sketch of magnetic field lines from the tunnel being drawn into the soft iron shield around the beam pipe. Note that due to the finite permeability of the iron, approximately 0.1% of the flux continues through to the beam.

When a layer of soft iron is wrapped around an otherwise non-ferric material such as the beam pipe, the higher permeability of the iron pulls magnetic flux lines from an area approximately double the width of the iron geometry. In the case of the Recycler, this covers an area almost 8" across. The plan is to use a layer of soft iron which is 6 mils thick. Therefore, the peak magnetic field in the soft iron is approximately 670 times larger than the ambient field. Since the saturation field of the soft iron is 20 kG, this puts an upper limit on the magnetic field at the Recycler of 30 Gauss. This is 5-10 times higher than anticipated. In specific locations in which there are known or discovered high magnetic field generating devices, extra shielding can be added to prevent the soft iron from going into saturation.

The problem with the above solution is that even when not in saturation, the soft iron has a finite permeability of approximately 3000-5000. Therefore, some fraction of the ambient tunnel magnetic flux still penetrates to the beam. For time-dependent fields the maximum level of attenuation is approximately 1000x. It is for this reason that mu-metal is inserted as an addition layer between the beam pipe and the soft iron.

The disadvantage of mu-metal is that it's saturation level is on 8 kG. On the other hand, it's permeability is in the range of 12,000-400,000. At fields up to 3 kG and frequencies up to 60 Hz, field attenuation factors of 100,000x are achievable [Amuneal Manufacturing Corp., "Complete Guide to Magnetic Shielding"]. The plan for the Recycler is to use a mu-metal layer which is 4 mil thick. Over basically the same area, the maximum residual field inside the soft iron which the mu-metal can shield is 2 Gauss. By design, this field matches the leakage expected through the soft iron just as it begins to seriously saturate.

The power spectrum of the magnetic fields in the tunnel below 60 Hz should be dominated by 0.5 Hz from the basic Main Injector ramp plus the first 10-100 harmonics needed to reproduce the more complex, non-sinusoidal current waveforms found in most correctors, busses, and specialty devices (such as Lambertsons). At these frequencies both the soft iron and mu-metal still behave as if exposed to a constant magnetic field.

2.6. RF System

The Recycler RF system which generates the longitudinal phase space gymnastics described in section 2.1 is composed of four 50Ω gaps driven by wideband amplifiers. The bandwidth of the net system is from 10 kHz to 100 MHz. The upper cutoff frequency corresponds to a voltage rise-time or fall-time of a few nanoseconds, far faster than actually necessary. The low frequency cutoff is composed of two poles, one from the gap inductance and the other from the amplifiers. Because there is no DC response in the system, two concerns need to be considered. The first is the amount of droop in the square voltage pulse during its duration. The second is the amount of baseline offset between the voltage pulses which can accelerate or decelerate beam particles which should be drifting.

The amount of droop can be calculated fairly easily. Using a simulation program to calculated response functions, as the two pole high pass filter response shown in figure 2.6.1, the resultant accelerating voltage waveform is presented in figure 2.6.2. For pulse lengths less than 1 µsec the droop is well less than 10%. This level of droop has only a small quantitative effect on the bucket height.

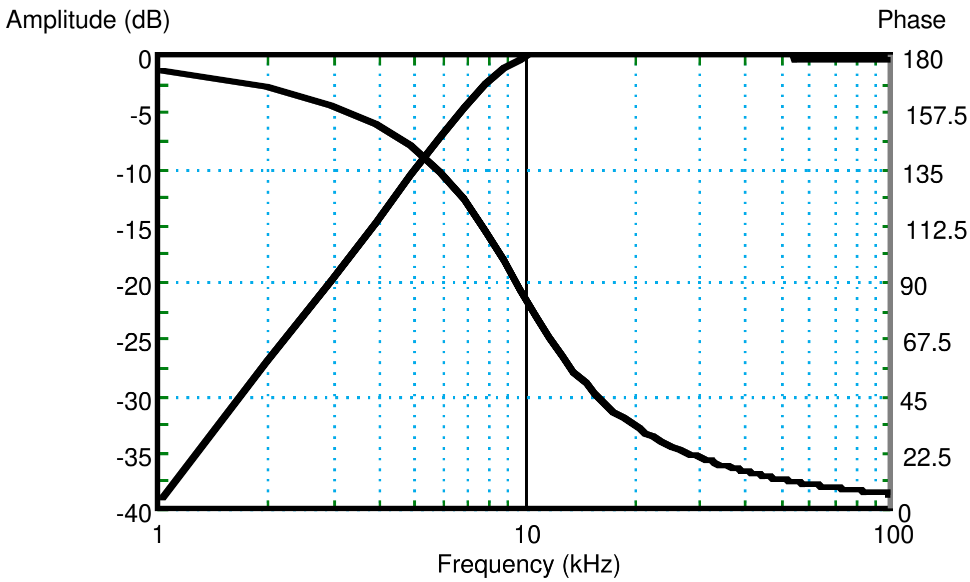

Figure 2.6.1: Two pole response function simulating the lower bandwidth limit of the accelerating gap and power supply.

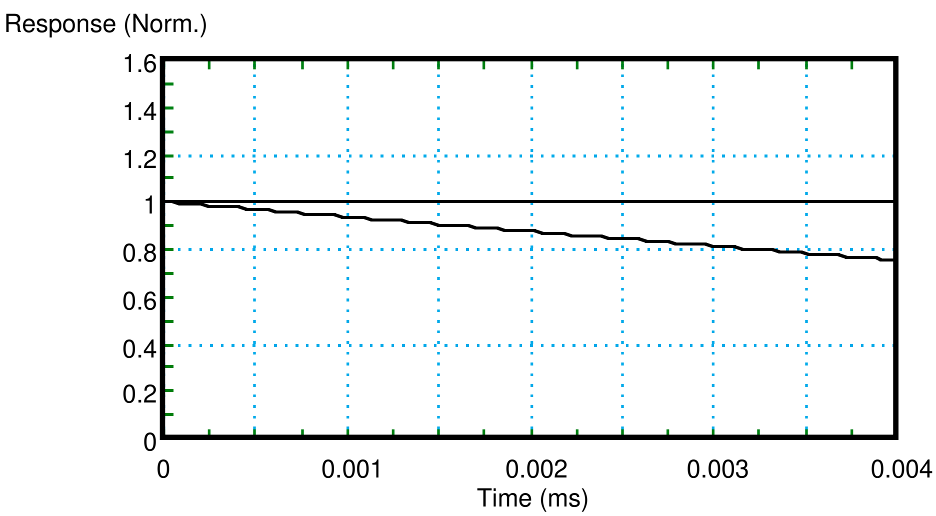

Figure 2.6.2: Calculation of the droop and the original pulse as a function of time. Note that for the most part pulse lengths of 1 μsec and less are envisioned, which infers that droops of less than 10% should be expected.

The first rule for suppressing baseline offsets is to always generate pairs of voltage pulses with equal and opposite areas, so that the net area is zero. This insures that there is no DC component in the drive signal. As can be seen in figure 2.6.3, after the pair of pulses the baseline voltage is at zero again. But note that inside the barrier bucket the drift region contains a nonzero residual voltage.

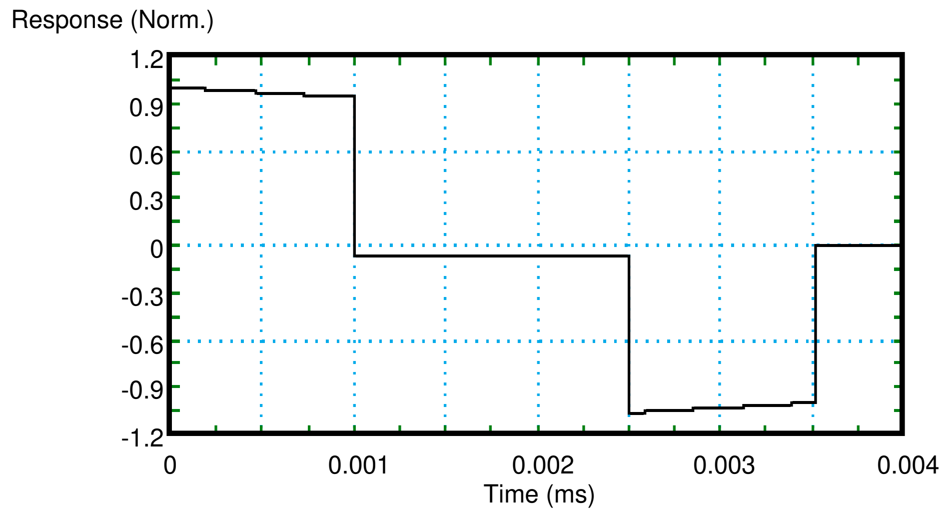

Figure 2.6.3: Calculation of the response to a barrier bucket pair constraining a 1.5 µsec batch with 1 µsec voltage pulses.

Another potential problem is the total impedance of 200Ω associated with the four gaps. The peak antiproton beam current envisioned is approximately 50 mA. Multiplying this current by the total impedance yields a beam loading waveform with a peak voltage of 10 V. Though this sounds like a small number, it is in fact enough to distort longitudinal phase space and cause a non-uniform beam distribution in the gap.

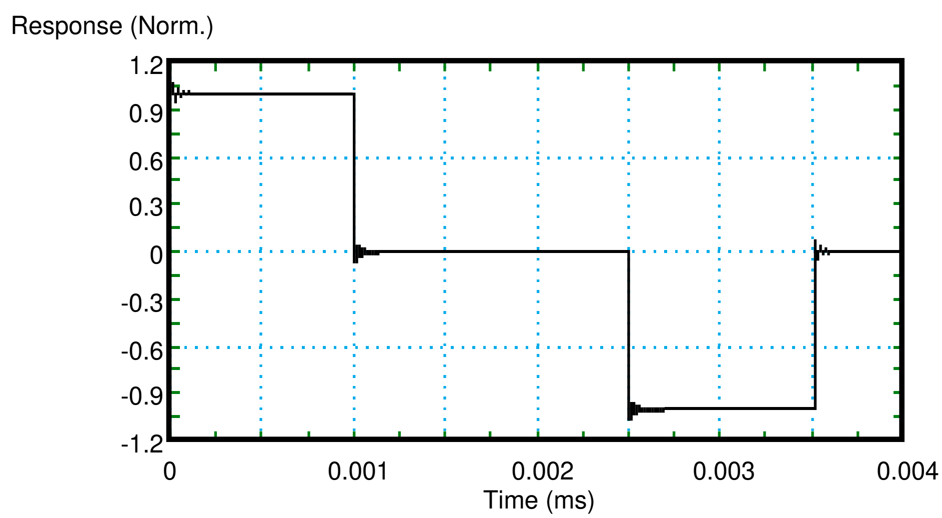

Figure 2.6.4: Calculation of the response to a barrier bucket pair constraining a 1.5 µsec batch with 1 µsec voltage pulses, but this time with a gap feedback system in operation with a loop gain of 10.

To fix the above three concerns simultaneously a feedback loop is envisioned. By comparing the gap voltage and the input to the amplifiers, the error signal is amplified and added back into the amplifier. In this way the errant voltage from the low frequency bandwidth limit and the beam loading voltage can be corrected. Figure 2.6.4 shows the result of the inclusion of such a feedback system with a loop gain of 10. Figure 2.6.5 contains a block diagram of the feedback system.

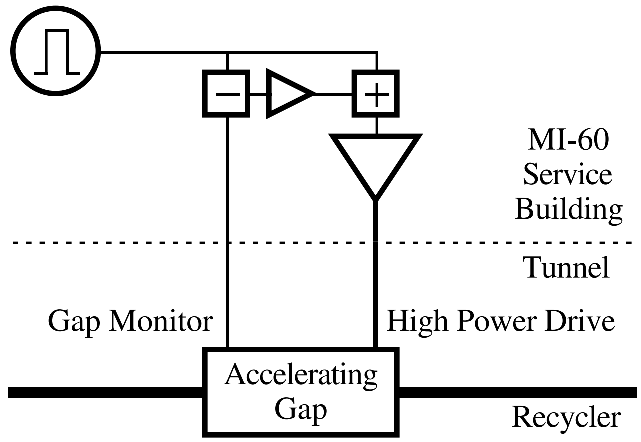

Figure 2.6.5: Block diagram of the feedback system around each gap/amplifier designed.

2.7. Impedances and Instabilities

Because the beam is unbunched, the instabilities which are expected to be a problem are not complicated. The two instabilities to be potentially concerned about are the transverse resistive wall instability and the longitudinal microwave instability.

2.7.1. Impedance Budget

The dominant sources of accelerator impedance in the Recycler ring are the beam position monitors, the kicker magnets, the accelerating cavities, and the resistance of the vacuum tube itself. At first one could assume that the impedance budgets of the Main Injector and the Recycler are the same at

$$\frac{Z_\parallel}{n} = 1.6\ \Omega \qquad Z_\perp = 2.2\ \mathrm{M}\Omega\,/\,\mathrm{m} \qquad .$$

However, the impedance will be dramatically less in the Recycler. For instance, there are no laminated Lambertson magnets, the kickers are slower and hence have a thicker coating, and there are no high-Q, high impedance RF cavities.

The beam impedance is dominated by the space-charge impedance. Calculation (K.Y. Ng) of the magnitude of this space charge impedance at a debunched beam intensity of $2.5\text{x}10^{12}$ yields the result

$$\frac{Z_\parallel}{n} = 12\ \Omega \qquad Z_\perp = 420\ \mathrm{M}\Omega\,/\,\mathrm{m}$$

2.7.2. Resistive Wall Instability

The resistive wall instability involves long wavelengths, and therefore does not depend on whether beam is bunched or coasting. Because the Recycler vacuum tube is the same material and cross-section as the Main Injector, the results obtained for the Main Injector for the instability growth time can simply be scaled with respect to the beam intensity. At an intensity of 1×10^{13} antiprotons, a growth time of approximately 3.6 ms, or 300 turns, is expected in the absence of space charge impedance or Landau damping. Note that a tune below the half integer was chosen to minimize the severity of the instability. Calculations including the space charge impedance and Landau damping indicate that the beam is in fact stable, and feedback systems are not necessary.

2.7.3. Microwave Instability

The minimum rms momentum spread in the Recycler will be 0.3 MeV. At that momentum spread the beam intensity is approximately 250×10^{10}. The threshold longitudinal impedance for microwave instability is given by

$$\left|\frac{Z_{\|}}{n}\right| < 0.68\pi \, Z_o \frac{|\eta|\gamma_r R}{N \, r_p}\left(\frac{\sigma_e}{E_o}\right)^2 \quad , \qquad (2.7.1)$$

where $r_p = 1.5 \times 10^{-18}$ m and Zo=377 Ω. Plugging in the rest of the numbers for the Recycler a threshold impedance of 70 Ω is found. The only impedance larger than this is from the four 50 Ω RF cavities at low frequencies below 1 MHz. If a problem did occur, the RF cavity feedback described above would suppress it.

2.8. Intrabeam Scattering

Intrabeam scattering, or Coulomb interaction between antiprotons, is the dominant heating mechanism which, when balanced against cooling forces from stochastic cooling, determines the equilibrium emittance achievable in the Recycler. Since each collision conserves energy, it is possible that as the thermal energy of one plane increases, which is related to the emittance in that plane, the emittance in another plane decreases, much as the temperatures of two heat reservoirs tend toward equilibrium. However, the potential for coupling some of the directed longitudinal beam energy into either longitudinal or transverse thermal motion in general leads to an overall increase in the phase space volume of the beam as a result of Coulomb interactions.

From simple kinematic arguments, it is possible to show that below transition, Coulomb collisions can lead to an equilibrium between the emittances of all planes, while above transition no such equilibrium is possible, that is, the emittance in all planes continues to increase. This comes about because the effective longitudinal temperature is proportional to the slip factor η, which implies a negative temperature above transition. The negative temperature is another manifestation of the negative mass instability.

Since the Recycler is well below transition, it could be expected that such an equilibrium is possible: i.e. the emittance of one plane increases while that of another decreases. However, this is only partly true due to two mitigating factors. First, since there is a distribution of energies and angles among colliding particles, the transition from equilibrium to growth conditions is gradual. A completely stationary equilibrium is only achievable at non-relativistic energies. Second, Mtingwa and Bjorken have shown that the overall phase space volume can only remain stationary if a specific condition on lattice parameters is satisfied everywhere which, in general, is usually never true for a given lattice. Stated in physical terms, whenever Coulomb scattering occurs in the presence of gradients, either in configuration or velocity space, work is effectively done on the distribution, namely, emittance growth occurs.

The original work on this subject was carried out by Piwinski, and later work, based on an alternative, but equivalent approach, was carried out by Mtingwa and Bjorken. The latter work is often cited, because of the generality of the analysis, however certain approximations are typically made in the literature which do not permit immediate application of this analysis to beams below transition. Using the most general expressions from these references, it can be shown there is still some discrepancy between Piwinski`s work and that of Mtingwa and Bjorken regarding the conditions necessary for thermal equilibrium. However, we have extensively studied these two formulations and have found that the quantitative differences between these models are small. In the following analysis, we assume there is no transverse coupling, and that all particle distributions are Gaussian.

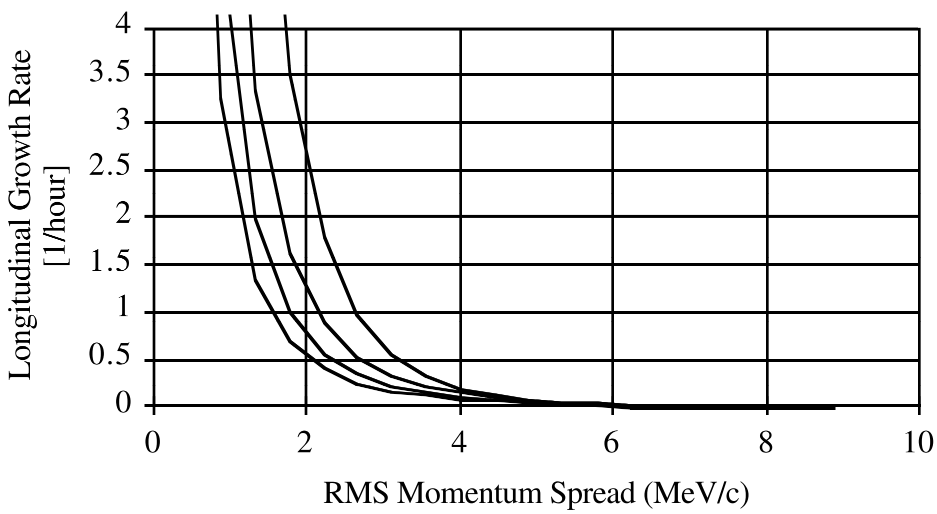

Figure 2.8.1: Longitudinal intrabeam scattering growth rates as a function of transverse emittance and momentum spread. The different curves are for transverse normalized 95% emittances of 5 (top), 10, 15, and 20 π mmmr (bottom). The beam intensity was 7×10^{12} antiprotons.

For the Recycler, there are two regimes of interest: a relatively high momentum spread regime in which stochastic cooling is used, and a regime with small where electron cooling is relevant. For large momentum spread, emittance growth times are shown in figure 2.8.1.

Inverse growth rates for the longitudinal plane are plotted as a function of momentum spread for various fixed transverse emittances (normalized, 95%). In figure 2.8.2, we plot the dependence of the horizontal scattering rates vs. momentum spread. At sufficiently small momentum spreads, it is possible that slight cooling of the horizontal emittance can occur through coupling to the relatively cold longitudinal plane. Note that since we have neglected coupling in this analysis, and there is no vertical dispersion, there is little coupling between the longitudinal and vertical planes. The vertical plane usually is cooled, but with very long cooling times. Hence it will be ignored in this analysis. In this regime, the sum of the horizontal and longitudinal inverse growth rates is approximately constant, although the net overall phase space volume increases, due to the presence of gradients. A small amount of longitudinal cooling is expected, as the transverse plane heats. In the limit of small momentum spread the situation is reversed where the longitudinal plane is strongly heated, while the horizontal plane can be measurably cooled.

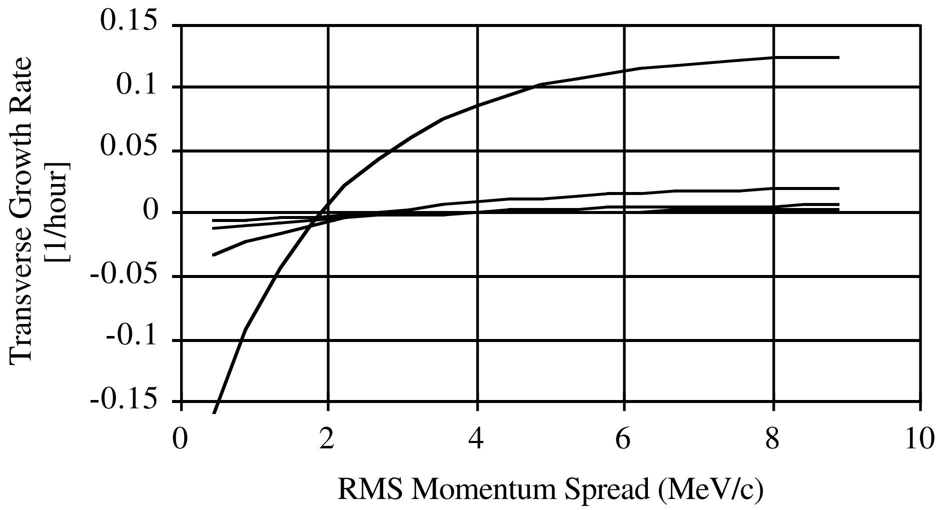

Figure 2.8.2: Transverse intrabeam scattering growth rates as a function of transverse emittance and momentum spread. The different curves are for transverse normalized 95% emittances of 5 (top on right edge), 10, 15, and 20 π mmmr (bottom on right edge). The beam intensity was $7\text{x}10^{12}$ antiprotons.

It should be noted that the actual equilibrium achieved is a balance between stochastic cooling and diffusion caused by scattering, all of which are non-Maxwellian processes; that is, tails will develop on the distributions as the energy-dependent diffusion and drag forces come to equilibrium in detailed balance. As such, the actual equilibrium must be found by the solution of a time-dependent Fokker-Planck approach.

It is worthwhile to note that the regime predicted for the Recycler in which some degree of transverse cooling is possible has not yet been investigated experimentally. It would be valuable to carry out a series of experiments in the Fermilab Accumulator, which can access the regime below transition.

2.9. Stochastic Cooling

The stochastic cooling systems in the Recycler ring are discussed in section 2.1 and chapters 3 and 4. The general picture one acquires is that the horizontal and vertical betatron cooling systems are not controversial and relatively straightforward. On the other hand, the momentum cooling system is critical, where cooling strength and momentum aperture are key design parameters. In this section the system parameters for both the betatron and momentum cooling systems are reviewed. To set the stage, the interaction between intrabeam scattering and stochastic cooling is explored explicitly first.

2.9.1. Intrabeam Scattering and Barrier Bucket Compression

The calculations of intrabeam scattering in the previous section indicate that the momentum growth rate for a fixed normalized 95% transverse emittance of 10 π mmmr is quite fast for the anticipated beam currents. In addition, the rate of increase in growth rate with diminishing rms momentum spread is very well described by the approximation

$$\alpha_{IBS} = \frac{k}{\left(\frac{\sigma_p}{P}\right)^3} \qquad , \qquad (2.9.1)$$

where $k=1.3\times10^{-11}$ hr^{-1} at an antiproton beam intensity of 7×10^{12}. Both the calculated and fit dependencies of intrabeam scattering growth rate on rms momentum spread are plotted in figure 2.9.1. Assuming a stochastic cooling/intrabeam scattering model in which distribution shapes are constant and rms momentum spread is an adequate parameterization of the beam temperature, a cooling system with a momentum cooling time of 1 hour can only reduce the rms momentum spread to approximately 2 MeV at the current of beam intensity of 7×10^{12}. The engineering form of the equation can be written as

$$\alpha_{IBS}[hr^{-1}] = 0.093 \frac{I_b\ [mA]}{\left(\sigma_E\ [MeV]\right)^3} \qquad , \qquad (2.9.2)$$

The cubic nature of the dependence of intrabeam induced growth time on rms energy spread suggests a Recycler stacking scenario in which the cooled beam distribution is always compressed in order to maintain the largest energy spread inside the energy aperture of the momentum cooling system. This time agile compression of the azimuthal distribution of the beam is carried out with the barrier bucket RF system.

Rough calculations [G. Jackson, MI-Note 164] indicate that a 0.5 hour momentum cooling time for a 21 mA instantaneous current antiproton beam with an rms energy spread of 2.7 MeV is sufficient for the beam distribution expected at any time in the Recycler ring during Run II.

As a result of the curve in figure 2.9.1, barrier bucket compression aimed at maintaining a large momentum spread at the expense of higher peak current will be systematically employed in the following scenario. Because of other side benefits, such as more efficient ion clearing due to the beam distribution gaps and the ease and flexibility of beam transfers, the RF system which generates these barrier voltage pulses is a key component in the Recycler.

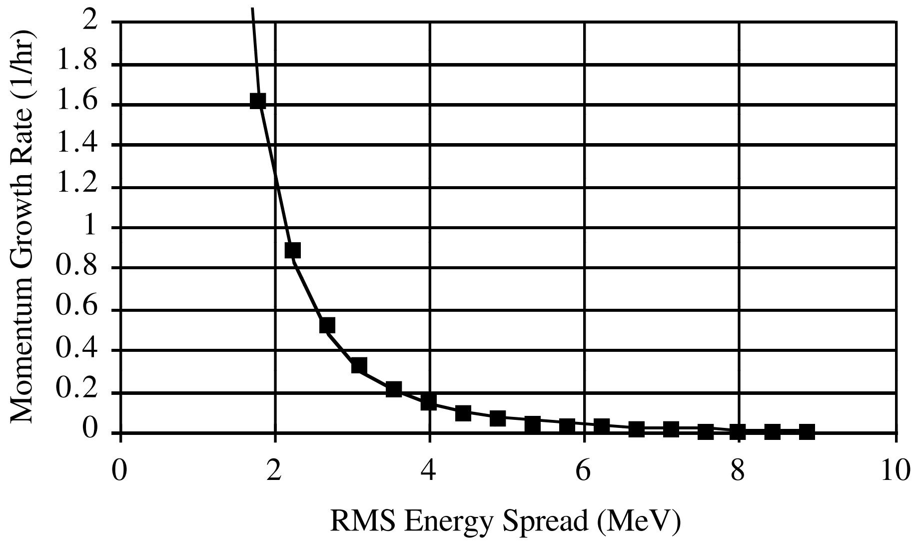

Figure 2.9.1: Calculated intrabeam scattering driven momentum growth rate in the Recycler ring as a function of momentum spread. The normalized 95% transverse emittance is 10 π mmmr and the antiproton intensity is 700×10^{10}. The points are calculated values while the line is the result of an inverse cubic fit.

2.9.2. General Considerations

The momentum cooling was chosen to be a filter cooling system. Non-overlapping Schottky bands are a requirement for this type of cooling system. The betatron cooling systems (horizontal and vertical) do not use any filters and the Schottky bands overlap slightly. The effect of these requirements is described in the section on Bandwidth below.

To minimize the phase errors in the cooling system ("bad mixing") the cooling signal is transmitted across the ring (from Q215 to Q111). Between these two locations particles traverse about 1/6 of the ring and accumulate approximately 1/6 of the phase slip. The signal will be transmitted with a modulated laser signal.

2.9.3. Bandwidth

The most important design choice concerns the system bandwidth. The maximum frequency that can be used without encountering Schottky band overlap is

$$\frac{\Delta p}{P} \eta f_{max} T_o \leq 1 \quad , \quad (2.9.3)$$

where

$$\eta = \frac{1}{\gamma_t^2} - \frac{1}{\gamma^2} \quad , \qquad (2.9.4)$$

γ_t is the Recycler relativistic transition energy, and γ is the relativistic beam energy. The revolution period T_o is determined mostly by the circumference of the Main Injector tunnel. The maximum cooling frequency f_{max} is therefore inversely proportional to the momentum spread.

The equilibrium momentum spread is determined by the balance between the cooling rate and the heating rate from external mechanisms. Intrabeam scattering is expected to be the dominant heating mechanism longitudinally. Since stacked beam is trapped between two RF barriers and both the cooling and heating rate depend on the separation between the barriers (barrier bucket compression), the momentum spread depends on the choice of the amount of bucket compression. However, the choice is limited by the necessity of retaining adequate longitudinal phase space for injecting and recycling antiprotons. For a given choice of bucket compression, the required momentum spread is determined by the need to maintain the loss from diffusion at a level that is small compared to the stacking rate. Calculations indicate that a momentum spread of ±20 MeV/c will adequately retain the beam with a cooling system bandwidth of 0.5 to 2.0 GHz. It is tentatively planned to achieve this bandwidth with two separate cooling systems: one operating from 0.5 to 1.0 GHz and one operating from 1.0 to 2.0 GHz.

The transverse cooling system limitation of the maximum frequency comes from the "bad mixing" between pickup and kicker. For a momentum spread of ±20 MeV/c a cooling bandwidth of 2.0 to 4.0 GHz is appropriate. The transverse heating rate from intrabeam scattering is quite small, and the transverse emittance will probably be determined by other mechanisms. It is probably undesirable for the transverse emittance to be smaller than 10π because of the increase in longitudinal intrabeam scattering that results from low emittance beams. On the other hand, the equilibrium emittance will not be much less than 10 π mmmr if the beam heating rate is 1 π mmmr/hr. For this reason, a maximum beam heating rate (from all sources other than the cooling system) has been specified to be a maximum of 1 π mmmr/hr.

2.9.4. Stability

The gain of the longitudinal cooling system is limited by stability considerations. It has been assumed that errors in the gain function will limit the gain to a value 10 dB below the stability limit. This assumption is thought to be somewhat (but not overly) conservative in light of experience with similar systems in the Antiproton Source.

The betatron cooling systems are stable well past the optimum gain and should not present any unusual stability problems.

2.9.5. Simulation Description

The simulation of the stacking process is derived from the Fokker-Planck simulation used to design the momentum cooling for the Antiproton Source. The simulation assumes a coasting beam and neglects the transverse motion. The line density in the simulation is computed from the total beam in the stack divided by the sum of the barrier bucket compression and 1/2 the pulse width. The RF stacking and unstacking are assumed to be perfectly adiabatic and with negligible emittance dilution. The bucket height (20 MeV) is treated as a hard aperture: particles that escape from the barrier bucket are lost.

Thus, the model used for the cooling process is exactly correct for a machine with an infinite voltage RF barriers and a finite momentum aperture. This model should be perfectly adequate for the dense portion of the antiproton stack. However, for particles that have larger momentum offsets, this approximation underestimates the time spent under the influence of the barrier and overestimates the particle density. For example, the stack is contained between two barrier voltage pulses that capture 139 eV-sec. The simulation, with infinite height buckets, contains only a total of 112 eV-sec.

Intrabeam scattering is incorporated in an average way with the addition of an energy independent diffusion constant

$$D = \frac{2\sigma_p^2}{\tau_I} \quad , \qquad (2.9.5)$$

where σ_p is the momentum of the beam and τ_I is the calculated intrabeam scattering heating time. The value of σ_p varies somewhat in the stacking process, but the variation is not included in the simulation. It is adequate to use the final value of σ_p. The value of D is, however, scaled to account for the changing intensity of the stored beam.

The system gain function is calculated using ideal components. Gain errors are introduced by multiplying the response function of a broad-band (Q=1) resonator centered at mid-band. No frequencies outside the nominal cooling band are considered: it is assumed that these frequencies contribute no net heating or cooling. The resulting gain functions are shown in figures 2.9.2 through 2.9.4.

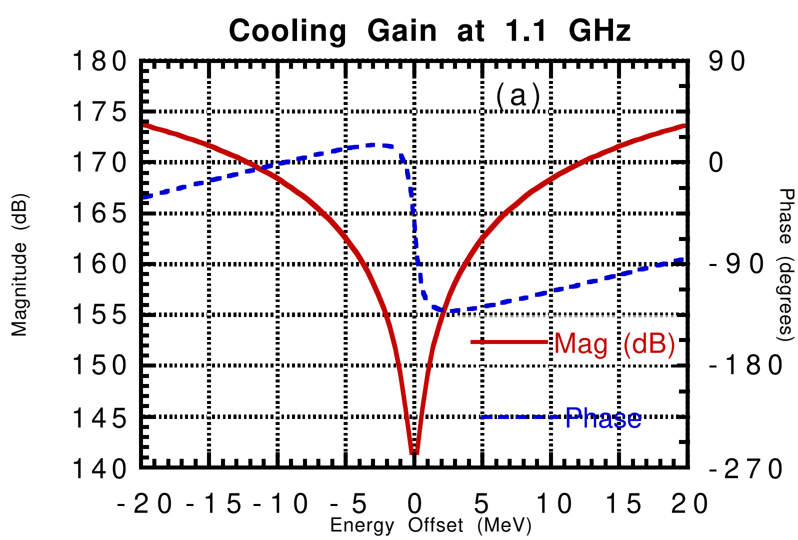

Figure 2.9.2: Momentum cooling gain functions for the Schottky band at 1.1 GHz.

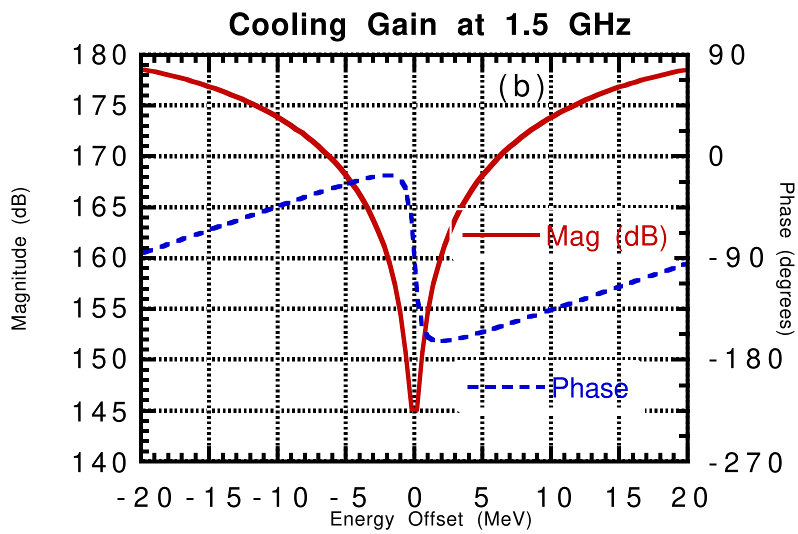

Figure 2.9.3: Momentum cooling gain functions for the Schottky band at 1.5 GHz.

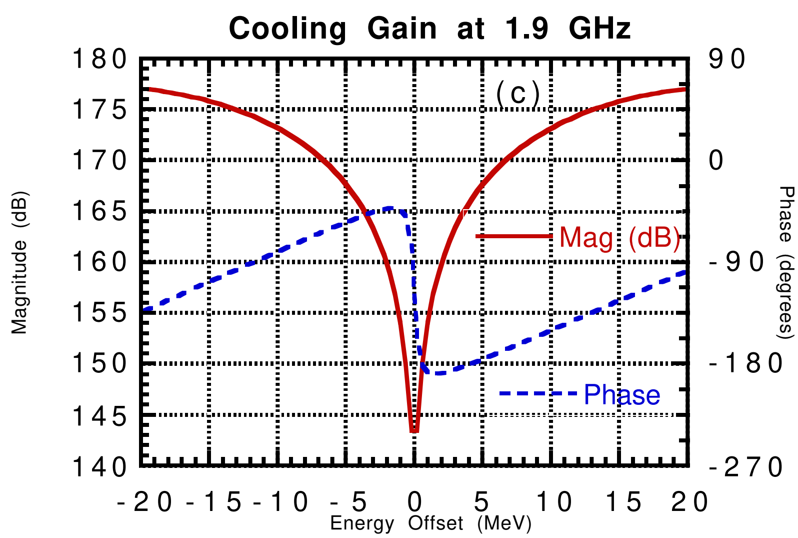

Figure 2.9.4: Momentum cooling gain functions for the Schottky band at 1.9 GHz.

The transverse cooling simulation is also based on a coasting beam approximation assuming that the particle momenta are constant. This assumption is not correct because: 1) the momentum cooling system changes the particle momenta, 2) the beam intensity and distribution changes as the beam is stacked, and 3) the RF changes the particle momenta. A proper calculation of the evolution of the distribution function would have to take into account both the longitudinal and transverse degrees of freedom. If, however, the distribution function can be written as a product of distribution functions for the longitudinal and transverse coordinates, the coasting beam approximation should be accurate. The momentum distribution is taken from the longitudinal stacking calculation and input to the transverse calculation. The transverse cooling is calculated for particles of a fixed momentum (but time varying density). Any new beam that is injected is assumed to have the same transverse distribution as the beam already present. The results of this calculation are shown below and are self-consistent with the above assumptions.

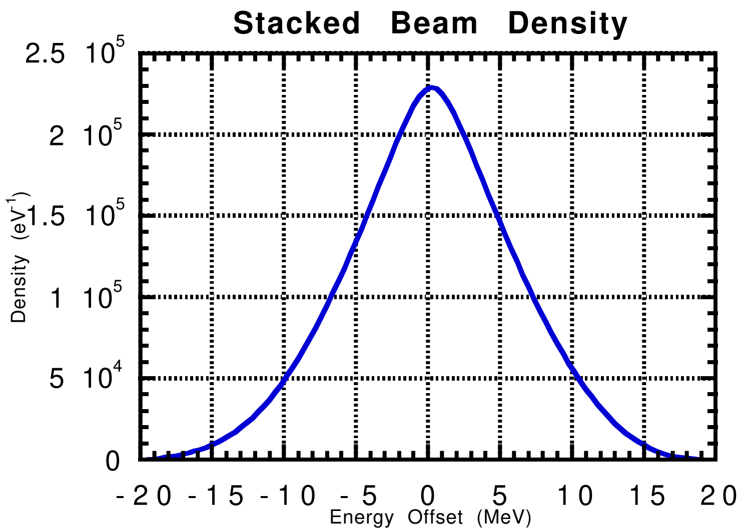

Figure 2.9.5: Longitudinal density profile obtained after 8 hours of stacking.

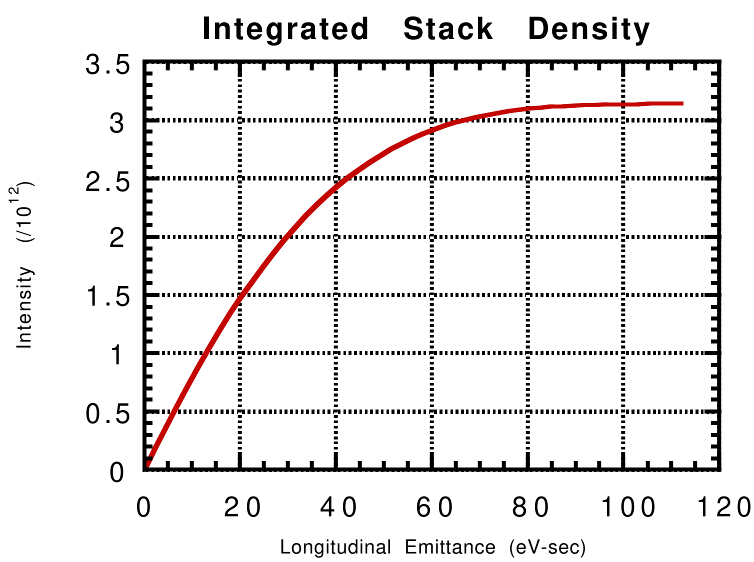

Figure 2.9.6: Integrated density profile obtained after 8 hours of stacking.

The transverse heating rate (from mechanisms other than the cooling systems) is critical. The simulation assumes that this rate is 1 π mmmr/hr. The longitudinal cooling system is specified to contribute less than 0.1 π mmmr/hr to the total.

2.9.6. Simulation Results

The final momentum distribution obtained is shown in figure 2.9.5. This distribution is integrated and shown in figure 2.9.6. As discussed above, the particle density is overestimated at high values of the momentum offset.

The stack size versus time in the cycle is shown in figure 2.9.7. Also shown is the cumulative stacking efficiency: the total stack size divided by the amount of beam injected in the current cycle. The maximum stack size is 3×10^{12} and the overall stacking efficiency for the cycle is about 98%.

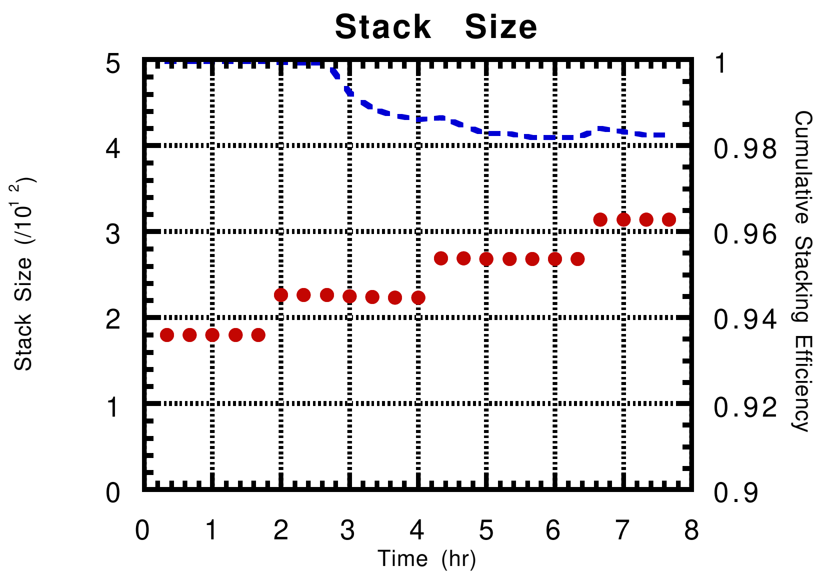

Figure 2.9.7: The stack size begins at t=0 at about $1.8\text{x}10^{12}$ antiprotons and grows to more than $3\text{x}10^{12}$ antiprotons after 7 hours of stacking. The cumulative stacking efficiency is equal to the current beam intensity divided by the sum of the initial beam and subsequent injections. The cumulative stacking efficiency exceeds 98% at the conclusion of the stacking cycle.

The simulation of the cooling of transverse emittance of the beam is shown in figure 2.9.8. The initial emittance of the beam is taken to be 30 π mmmr (100%). The beam cools rapidly initially and then grows as the intensity increases and the cooling rate decreases. The fraction of the beam that is contained within the 10 π mmmr emittance design goal is shown in figure 2.9.9. At the conclusion of the 8 hour stacking cycle virtually all of the beam is within this emittance.

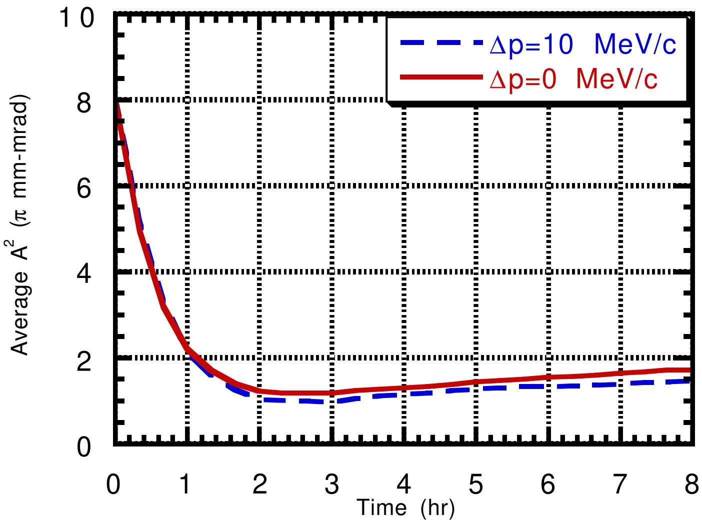

Figure 2.9.8: The evolution of the average amplitude-squared of the beam betatron motion. The beam emittance (95%) is approximately 3x the average amplitude-squared. The recycled beam cools rapidly initially until it reaches a minimum after which it grows because of the increasing intensity.

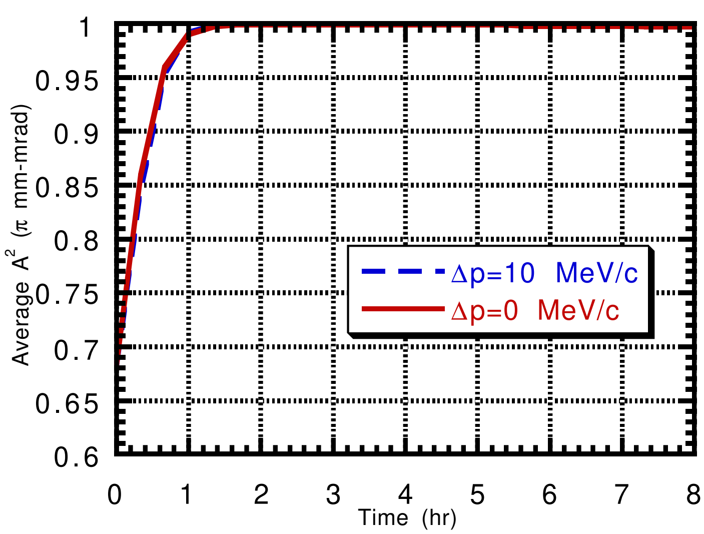

Figure 2.9.9: The fraction of the beam contained in a 10 π mmmr emittance (100%). The fraction becomes nearly 100% after 2 hours of cooling.

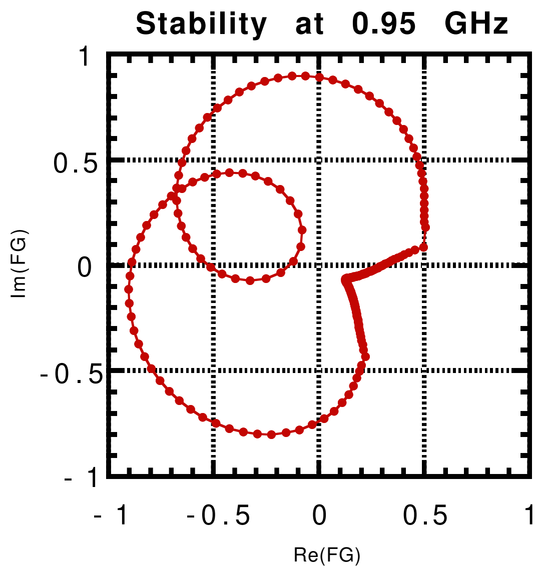

Figure 2.9.10: Stability diagram for the Schottky bands at 0.95 GHz at 7:40 (just before transfer to the Tevatron). The curve is a parametric plot of the real versus imaginary parts of the product gain (G) and beam feedback (F) functions. The points are spaced at 0.4 MeV intervals. The gain has been chosen so that the curve crosses the real axis at 0.3.

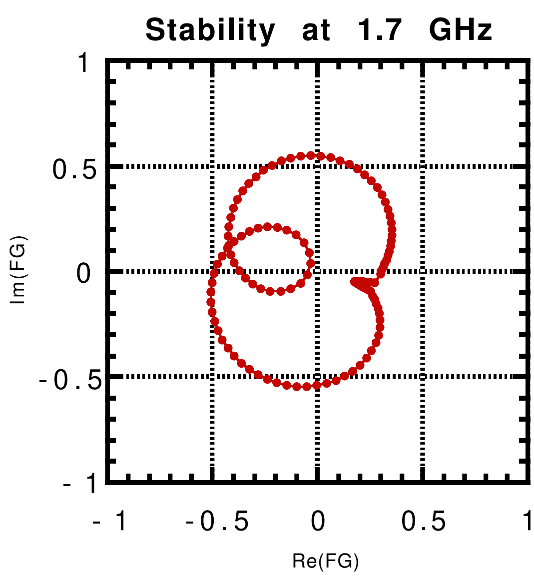

Figure 2.9.11: Stability diagrams for the Schottky bands at 1.7 GHz at 7:40 (just before transfer to the Tevatron). The curve is a parametric plot of the real versus imaginary parts of the product gain (G) and beam feedback (F) functions. The points are spaced at 0.4 MeV intervals. The gain has been chosen so that the curve crosses the real axis at 0.3.

The stability diagrams for the two momentum cooling system bands are shown in figures 2.9.10 and 2.9.11 for the time 7:20 - just before transfer to the Tevatron. This case is the one with the lowest stability margin. The stability criterion is that the curve cross the real axis with an intercept less than 1. The gain function has been scaled in the simulation so that the stability curve passes through the point (0.30,0.0). The stability margin, particularly in the lower band, is sensitive to phase errors in the gain function. However, it is believed that the designed stability margin is large enough that unanticipated phase errors can be tolerated.

The stability criterion as stated is actually unduly restrictive in that it is sufficient but not necessary. However, the more general stability criterion is not of practical importance for these systems.

2.9.7. Specifications: Longitudinal

The specifications for the momentum cooling system are given in Table 2.9.1.

Table 2.9.1: Momentum Cooling System Specifications

	Band 1	Band 2	
Pickups (PU)			
Beta Function at PU	35	35	m
Beam Transverse Emittance	10	10	π mmmr
Beam Size	22.68	22.68	mm
Number of Pickups	16	32	
PU Impedance	100	100	Ω
PU Gap	30	30	mm
Pickup Width	40	40	mm
PU Sensitivity	0.84	0.84	
PU Combiner Loss Factor	2	2	dB
Number of Tanks	1	1	
PU Repeat Length	12	7	cm
Overall Tank Length	2.32	2.64	m
Electronics			
Lower Frequency	0.5	1	GHz
Upper Frequency	1	2	GHz
Maximum Noise Figure	1	1	dB
Nominal Pickup Temperature	293	293	°K
Nominal Electronic Gain	116	101	dB
Notch Depth	30	30	dB
Notch Dispersion	20	20	ppm
Max Gain Ripple (Small Scale)	10	10	dB
Max Gain Variation (Large Scale)	3	3	dB
Nominal Noise Power	2	2	W
Nominal Schottky Power	6	3	W
Nominal Total Power	8	5	W
Amplified Rated (Saturated) Power	100	100	W
Kickers			
Number of Kickers	16	32	
Kicker Impedance	100	100	Ω
Kicker Gap	30	30	mm
Kicker Width	40	40	mm
Kicker Sensitivity	0.84	0.84	
Kicker Loss Factor	2	2	dB
Number of Kicker Tanks	1	1	
Overall Tank Length	2.32	2.64	m
Maximum Transverse Growth Rate	0.1	0.1	π mmmr/hr

2.9.8. Specifications: Transverse

The specifications for the betatron cooling systems are given in Table 2.9.2.

Table 2.9.2: Transverse Cooling System Specifications

Pickups (PU)		
Beta Function at PU	35	m
Beam Transverse Emittance	10	π mmmr
Beam Size	22.68	mm
Number of Pickups	32	
PU Impedance	100	Ω
PU Gap	30	mm
Pickup Width	22.5	mm
PU Sensitivity	0.83	
PU Combiner Loss (2 GHz)	2	dB
PU Combiner Loss (4 GHz)	2	dB
Number of Tanks	1	
PU Repeat Length	4.5	cm
Overall Tank Length	1.84	m
Electronics		
Lower Frequency	2	GHz
Upper Frequency	4	GHz
Maximum Noise Figure	1	dB
Nominal Pickup Temperature	293	°K
Electronic Gain	86	dB
Max Gain Ripple (Small Scale)	10	dB
Max Gain Variation (Large Scale)	3	dB
Nominal Noise Power	0	W
Nominal Schottky Power	2	W
Nominal Total Power	2	W
Maximum (Saturated) Power	50	W
Kickers		
Beta Function @ Kicker	35	m
Number of Kickers	32	
Kicker Impedance	100	Ω
Kicker Gap	30	mm
Kicker Width	22.5	mm
Kicker Sensitivity	0.62	
Kicker Loss(2 GHz)	2	dB
Kicker Loss(4 GHz)	2	dB
Number of Kicker Tanks	1	
Overall Tank Length	1.84	m